Contribution to a geodynamic reconstruction of the Anti-Atlas (Morocco) during Pan-African times with the emphasis on inversion tectonics and metallogenic activity at the Precambrian–Cambrian transition

Dominique Gasquet [a,*], Gilles Levresse [b], Alain Cheilletz [c], Moulay Rachid Azizi-Samir [d], Abdellah Mouttaqi [e]

[a] *Université de Savoie, CISM-EDYTEM, CNRS-UMR 5204, Campus Scientifique, 73376 Le Bourget du Lac Cédex, France*
[b] *UNAM, Centro de Geociencias, Campus Juriquilla, 76230 Santiago de Queretaro, Mexico*
[c] *CRPG-CNRS UPR A2300 and ENSG-INPL, BP 20, 54501 Vandoeuvre-lès-Nancy Cédex, France*
[d] *Reminex, Groupe ONA, 26 Av. Allal El Fassi, Tissir 36-40, Marrakech, Morocco*
[e] *ONHYM, 5 Charia My Hassan, BP 99, Rabat, Morocco*

Abstract

New geochronological analyses (U–Pb SIMS zircon ages) have yielded ages of 552 ± 5 Ma for the Bou Madine rhyolitic dome (Ougnat, eastern Anti-Atlas), 543 ± 9 Ma for the Tachkakacht rhyolitic dyke (Saghro–Imiter, eastern Anti-Atlas), and 531 ± 5 Ma for the Aghbar trachytic sill (Bou Azzer, central Anti-Atlas). Inherited zircon cores from the Aghbar trachytic sill and from the Bou Madine rhyolitic dome have been shown to be of Statherian age (ca. 1600–1800 Ma) and Palæoproterozoic (>2100 Ma) age, respectively, suggesting that a significantly older protolith underlies the Pan-African rocks in the Central and Eastern Anti-Atlas. Granodiorites and rhyolites from the Saghro–Imiter area have similar low $^{87}Sr/^{86}Sr$ (0.702–0.706) and $^{143}Nd/^{144}Nd$ (0.5116–0.5119) initial ratios, suggesting a mixture of mantle and lower crust sources. This can also be inferred from the low $^{187}Os/^{188}Os$ ratios obtained on pyrite crystals from the rhyolites.

A recently published lithostratigraphic framework has been combined with these new geochemical and geochronological data, and those from the literature to produce a new reconstruction of the complex orogenic front that developed at the northern edge of the Eburnian West African craton during Pan-African times. Three Neoproterozoic magmatic series can be distinguished in the Anti-Atlas belt, i.e., high-K calc-alkaline granites, high-K calc-alkaline to shoshonitic rhyolites and andesites, and alkaline-shoshonitic trachytes and syenites, which have been dated at 595–570, 570–545 and 530 Ma, respectively.

The accretion of the Pan-African Anti-Atlas belt to the West African super continent (WAC) was a four-stage event, involving extension, subduction, moderate collision and extension. The calc-alkaline magmatism of the subduction stage was associated

* Corresponding author. Tel.: +33 3 79 75 86 45; fax: +33 3 79 75 87 77.
E-mail address: dominique.gasquet@univ-savoie.fr (D. Gasquet).

with large-scale base metal and gold mineralisation. Metallogenic activity was greatest during the final extensional stage, at the Precambrian–Cambrian boundary. It is characterised by world-class precious metal deposits, base–metal porphyry and SEDEX-type occurrences.

1. Introduction

The geodynamic reconstruction of ancient belts is extremely important for understanding the development of ore deposits, particularly those associated with metal-concentration systems that involve parts of the lower crust and mantle and are therefore able to develop large-tonnage, high grade ore deposits (Ord et al., 1999; Kay and Mpodozis, 2001). In order to reconstruct complex and long-lived orogenic fronts and to understand some of the fundamental processes (on a lithospheric scale) involved in the production of large mineral concentrations, it is necessary to have geological data for a whole region, particularly geophysical and geochemical data, supported by solid geochronological and structural data. This paper focuses on the Neoproterozoic evolution of the Anti-Atlas Mountains (AA) of Morocco, a segment of the Pan-African chain that developed along the northern edge of the West African Craton (WAC). The region houses large world-class ore deposits (Fig. 1) and known reserves have recently been increased by new discoveries made during extensive exploration programs carried out as part of the ambitious National Geological Mapping Project funded by the Moroccan Ministry of Energy and Mines. One of the most important results of this project has been to improve our understanding of metallogenic activity during the 300 Ma-long Neoproterozoic history of the Anti-Atlas. For example, geochemical data produced during a recent study of the Imiter Ag–Hg deposit (stock metal estimated at 8000 metric tonnes Ag[0]) clearly show a large-scale transfer of chalcophile elements from the mantle to superficial (km-deep) crustal levels (Levresse et al., 2004). It is also essential to draw up precise and reliable lithostratigraphic sections through the orogenic belt, taking into account new geochronological data, in order to accurately define the architecture of the chain. This paper combines new U/Pb geochronological and geochemical data from the Bou Azzer, Saghro–Imiter and Ougnat–Bou Madine inliers (Eastern AA) with a discussion of results published by other workers in order to propose a clearer picture of this Neoproterozoic orogenic belt. The discussion focuses on the final stages of the geodynamic evolution of the Pan-African Anti-Atlas belt, as this period is fundamental to the understanding of the northern border of the WAC and its metallogenic activity.

2. Geological setting of the Anti-Atlas belt of Morocco

The Moroccan Anti-Atlas belt is situated on the northern edge of the Eburnian (ca. 2 Ga) West African Craton (Fig. 1); it is separated from the High Atlas and the Mesetian domains to the north by the South Atlas Fault. The Anti-Atlas region was slightly reworked by the Hercynian and Alpine orogenies (Piqué, 1994; Caritg et al., 2004), which had a profound influence on the Meseta-Atlas domains. In the High Atlas domain, at Tamlelt in the East (Du Dresnay, 1976; Houari and Hoepffner, 2003) and in the western part of the High Atlas (Baouch, 1984; Ouazzani et al., 2001; Eddif, 2002), blocks of Precambrian materials were moderately deformed by the Variscan and Alpine tectonics. The original position of these blocks is still subject to debate and it is uncertain whether they belong to a hypothetical North Moroccan continent (Villeneuve and Cornée, 1994), to Avalonian–Cadomian terranes (Ennih and Liégeois, 2001), or to Carolina–Iberia terranes (Piqué, 2003). In the Anti-Atlas, the Precambrian basement comprises several units of Palæoproterozoic to Late Proterozoic age, unconformably overlain by late Ediacaran to Cambrian rocks and then by mostly sedimentary Palaeozoic rocks. The Precambrian basement outcrops in several inliers within late Ediacaran and younger units (Bas Drâa, Ifni, Kerdous, Akka, Igherm, Sirwa, Zenaga, Bou Azzer, Saghro and Ougnat; Fig. 1) distributed along two major fault zones (South Atlas
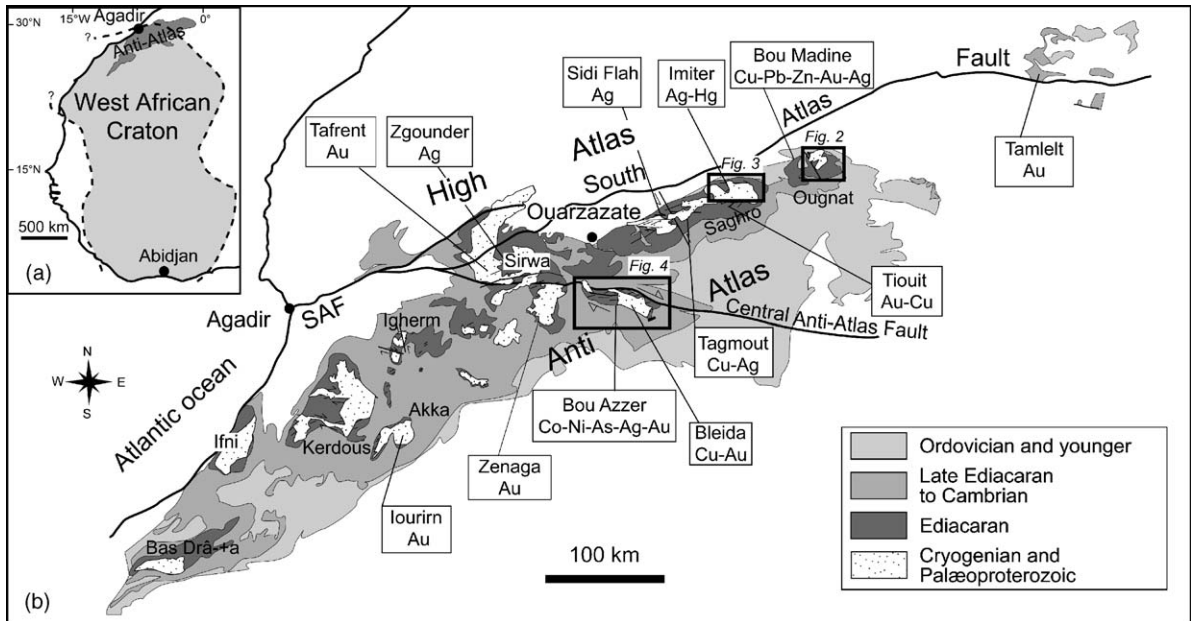
Fig. 1. (a) The Anti-Atlas belt at the northern limit of the West African craton, redrawn after Dallmeyer and Lecorché (1991). (b) Geological sketch map of the Anti-Atlas belt in southern Morocco and location of main ore deposits. SAF: South Atlas Fault.

Fault, and Central Anti-Atlas Fault; Fig. 1). Due to the extent of its sedimentary cover, for a long time the structure and tectonic evolution of the Pan-African Anti-Atlas belt was poorly understood, but now a basic consensus on the major stages of its development has been reached. Two main periods of tectono-thermal magmatic activity, associated with crustal accretion, have been recognised: (i) a Palæoproterozoic period, corresponding to the Eburnean (Birimian) orogeny, (ii) a Neoproterozoic period, corresponding to the Pan-African orogeny. Most authors (Leblanc and Lancelot, 1980; Bassias et al., 1988; Leblanc and Moussine-Pouchkine, 1994; Villeneuve and Cornée, 1994; El Aouli et al., 2001; Ennih and Liégeois, 2001; Fekkak et al., 2001; Thomas et al., 2002; Piqué, 2003; Gasquet et al., 2004) consider that the development of the Pan-African orogen can be explained by a three-stage process controlled by crustal extension, followed by compression, and then by a second extension stage. (1) The first stage was related to the rifting and break-up of the West African Craton and involved the successive development of an oceanic plateau, an island arc and a marginal basin, with associated blue-schist metamorphism (ca. 800–690 Ma; Clauer,

1974; Hefferan et al., 2002). Whether the subduction plane associated with island arc development dipped north or south is still unclear. (2) The second stage (ca. 690–605 Ma) is characterised by basin closure, southward directed arc–continent collision (arc accretion), ophiolite obduction, deformation, metamorphism and calc-alkaline magmatism. This convergence episode was associated with a southward dipping subduction plane. (3) The final, post-collision extension stage (605–530 Ma) is characterised by molasse sedimentation and magmatism, which was followed by the foreland development of the Saharan cratonic basin to the south. The Statherian (ca. 1750 Ma) and Variscan (ca. 300 Ma) events did not have a major effect on the AA except in its western part (Gasquet et al., 2004), where the Variscan shortening is expressed by polyharmonic buckle folding in the Palæozoic sedimentary cover. The Precambrian basement was only subject to faulting (Helg et al., 2004; Caritg et al., 2004).

The new geochronological data we have obtained for three selected inliers have allowed us to clarify the description of the post-collision extensional stage of the Pan-African orogeny.

3. Geological setting of the Ougnat, Saghro and Bou Azzer inliers

3.1. Ougnat–Bou Madine

Cryogenian to early Ediacaran schistose greywackes and black shales (Saghro Group) outcrop in the centre of the Bou Madine inlier (Fig. 2, after Freton, 1988). They are metamorphosed to greenschist facies and intruded by quartz-diorites and garnet-bearing granites, the ages of which have not been geochronologically established (Abia et al., 2003). This basement is unconformably overlain by Ediacaran volcanic formations (Ouarzazate Supergroup), which mostly consist of ignimbrites and minor andesites, with basaltic lava flows at the top. Moreover, in the Bou Madine area, the ignimbrites have been intruded by several rhyolitic domes and numerous felsic dykes. One of the Ediacaran rhyolitic domes is associated with polymetallic Zn–Cu–Pb–Sn–Ag–Au mineralisations. These mineral deposits occur in NNW–SSE en-echelon vein arrays related to Ediacaran transcurrent tectonics represented by N30°E strike-slip fault zones (Freton, 1988; Aït Saadi, 1992; Abia et al., 1999, 2003). A Cambrian sedimentary cover sequence unconformably overlies the Neoproterozoic rocks.

3.2. Saghro–Imiter

In the Imiter area (Fig. 3), the oldest sedimentary rocks are represented by Cryogenian sequences of black shales (Saghro Group), interpreted as having formed in an extensional back-arc environment (Marini and Ouguir, 1990; Ouguir et al., 1996). These rocks were folded and subject to low greenschist facies metamorphism during the main Pan-African event. The black shales are unconformably overlain by an Ediacaran volcanic and volcanoclastic sequence (Ouarzazate Supergroup), with compositions that range from andesitic at the bottom to ignimbritic at the top. This sequence hosts the Imiter Ag–Hg deposit, which is now considered to be of epithermal origin (Cheilletz et al., 2002; Levresse et al., 2004). The silver mineralisation is genetically related to a series of felsic volcanics (Takhatert calc-alkaline rhyolitic dome), which were coeval with regional extensional tectonics (Levresse, 2001). These volcanics have been dated at 550 ± 3 Ma by ion-probe U/Pb on zircons (Cheilletz et al., 2002). This epithermal event postdates an earlier discrete base metal episode associated with intrusive granodiorites (Taouzzakt, Igoudrane; Fig. 3), dated at 572 ± 5 Ma (Cheilletz et al., 2002). These calc-alkaline intrusive rocks produced a cordierite-andalusite-biotite contact-metamorphism assemblage in the country rocks (Leistel and Qadrouci, 1991; De Wall et al., 2001). Dykes of intermediate composition (mostly trachyandesite) and of various relative ages are present along the Ediacaran Imiter normal fault zone.

The felsic dykes, including the Tachkakacht dyke, are similar in composition to the Takhatert dome. Middle Cambrian sedimentary rocks overly the Neoproterozoic rocks. The Variscan and Alpine orogenies, although active in various sections of the AA belt, are thought to have had little effect in the Imiter area (Ouguir et al., 1994).

3.3. Bou Azzer–Aghbar

The Bou Azzer inlier (Fig. 4) is structurally the most complex part of the whole Anti-Atlas (see Leblanc, 1981; Saquaque et al., 1989, 1992). A Palæoproterozoic basement, including gneisses, amphibolites, and schists, is intruded by granites and overlain by Cryogenian formations (Bou Azzer Group) comprising (i) epicontinental sedimentary and volcanoclastic rocks and (ii) a mafic–ultramafic complex, interpreted as an ophiolite (Leblanc, 1975; Brabers, 1988), comprising serpentinites, gabbros, quartz-diorites and mafic volcanics, and associated with limestones, quartzites and sandstones. These formations were deformed by the main Pan-African shortening tectonic event (thrusts) and are unconformably overlain by, successively: (i) the molassic Tiddiline Group, (ii) the Ediacaran Ouarzazate Supergroup, which consists of a thick (∼1000 m) volcano-clastic pile (dacitic to rhyolitic ignimbrites, andesites, conglomerates, sandstones, etc.) emplaced during strong transtensive tectonics (Maacha et al., 1998), and (iii) the late Ediacaran to early Palæozoic Taroudant Group (dolomites, sandstones and rare sills of syenite and trachyte at Jbel Boho and Aghbar). The regional N–S shortening that occurred during the Variscan orogeny (Soulaïmani et al., 1997; Belfoul et al., 2001; Caritg et al., 2004) reactivated the major Eburnean and Pan-African faults. A complex, telescoped, polymetallic (Co–Ni–As–Fe–Cu–Au–Ag)
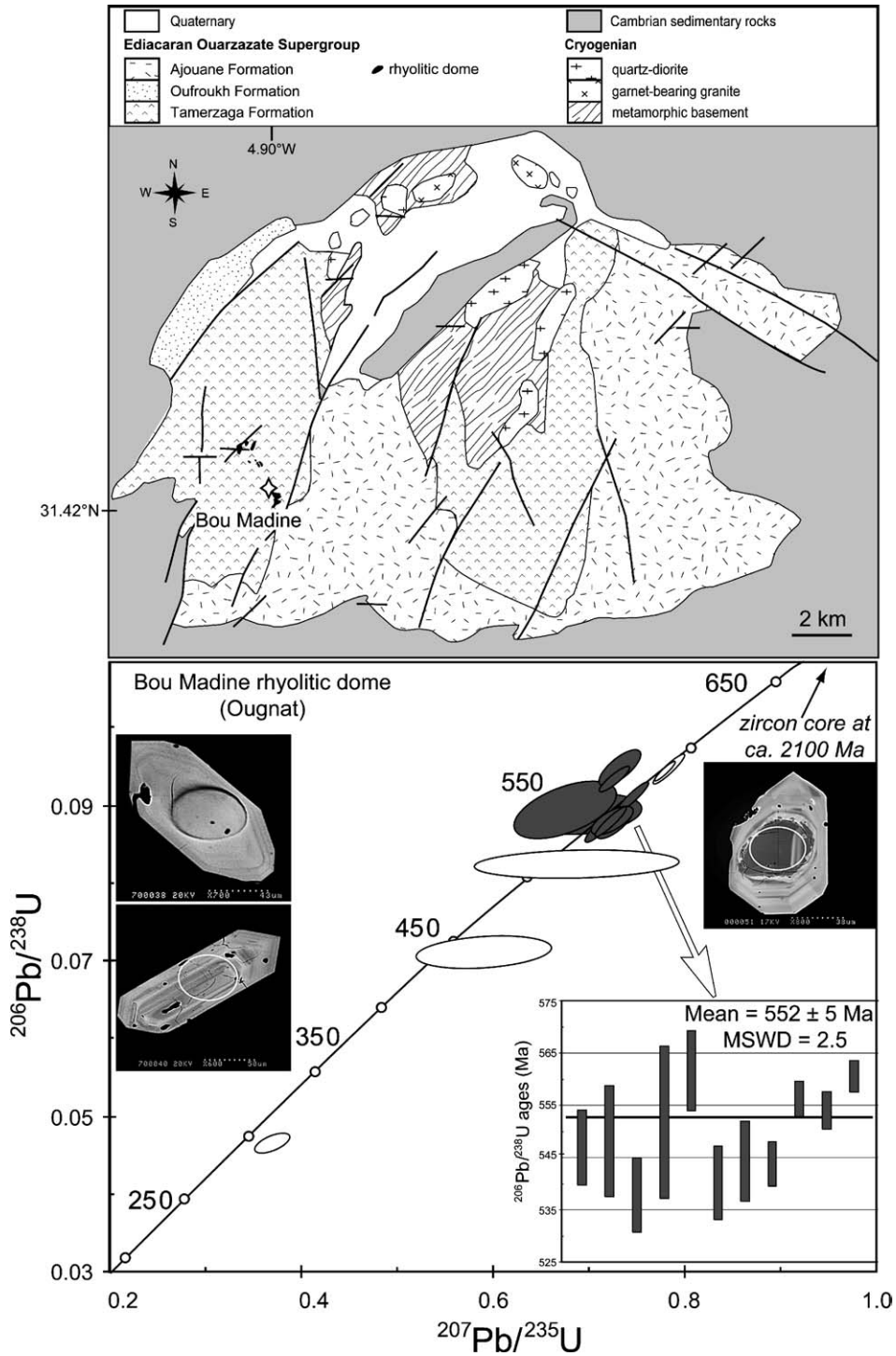
Fig. 2. Main geological units of the Ougnat–Bou Madine inlier (after Freton, 1988) and concordia diagram for zircons from the Bou Madine rhyolitic dome. Weighted mean ages, ellipses are 2σ errors. Star represents the position of the dated rhyolite.
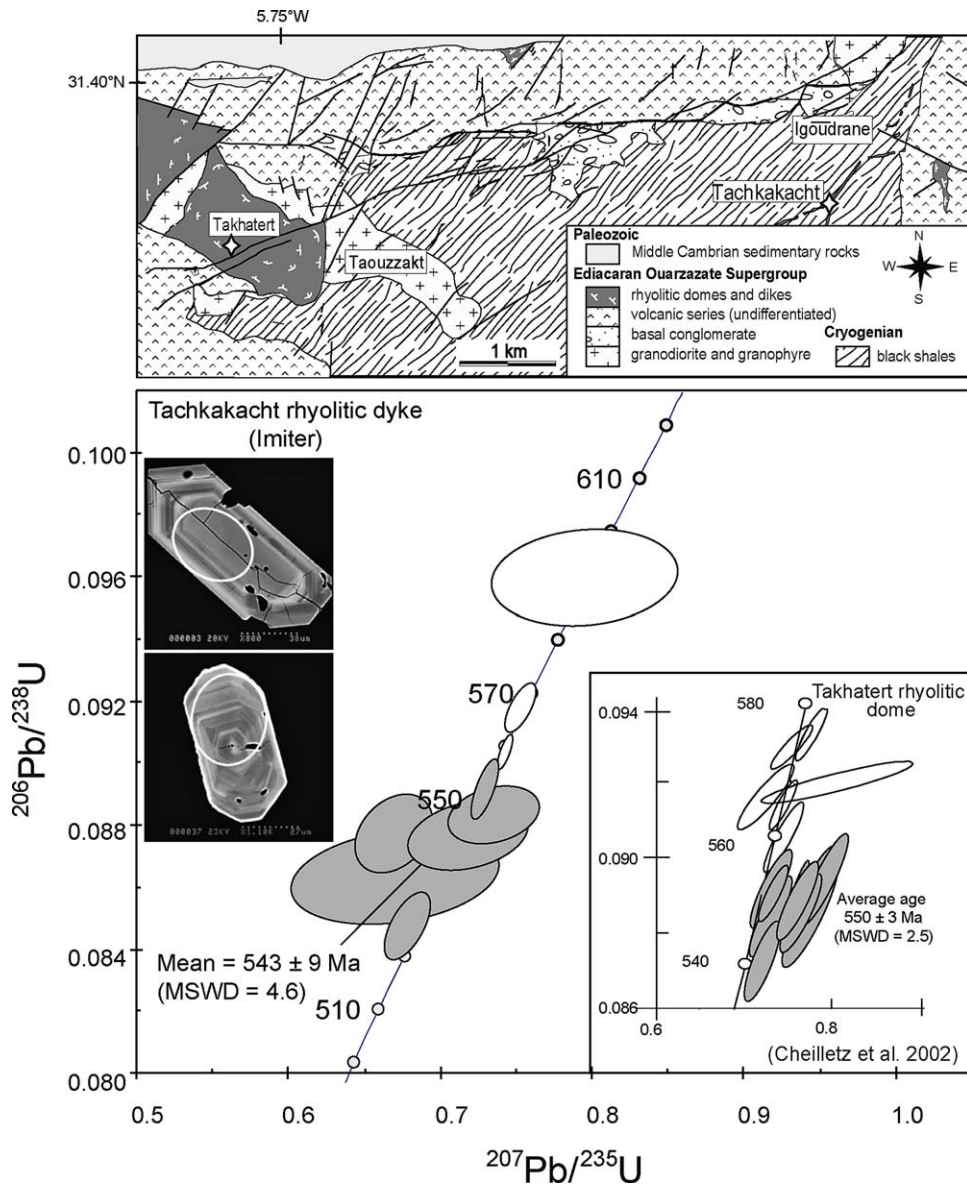
Fig. 3. Main geological units of the Saghro–Imiter inlier (after Leistel and Qadrouci, 1991; Levresse, 2001) and concordia diagram for zircons from the Tachkakacht rhyolitic dyke and (inset) the rhyolitic Takhatert dome (Cheilletz et al., 2002). Weighted mean ages, ellipses are 2σ errors. Stars represent the position of the dated rhyolites.

mineral deposit was formed during these Pan-African and Variscan events (Maacha et al., 1998). The age of the mineralisation is poorly constrained at 550 Ma by U–Pb dating on brannerite (En-Naciri et al., 1997) and at 218 ± 8 Ma by $^{40}Ar/^{39}Ar$ dating on hydrothermal muscovites (Levresse, 2001).

4. U–Pb geochronology in the Ougnat, Saghro and Bou Azzer inliers

4.1. Analytical procedures

U–Pb data were obtained for single zircon grains from Ouarzazate and Taroudant Group volcanic rocks.
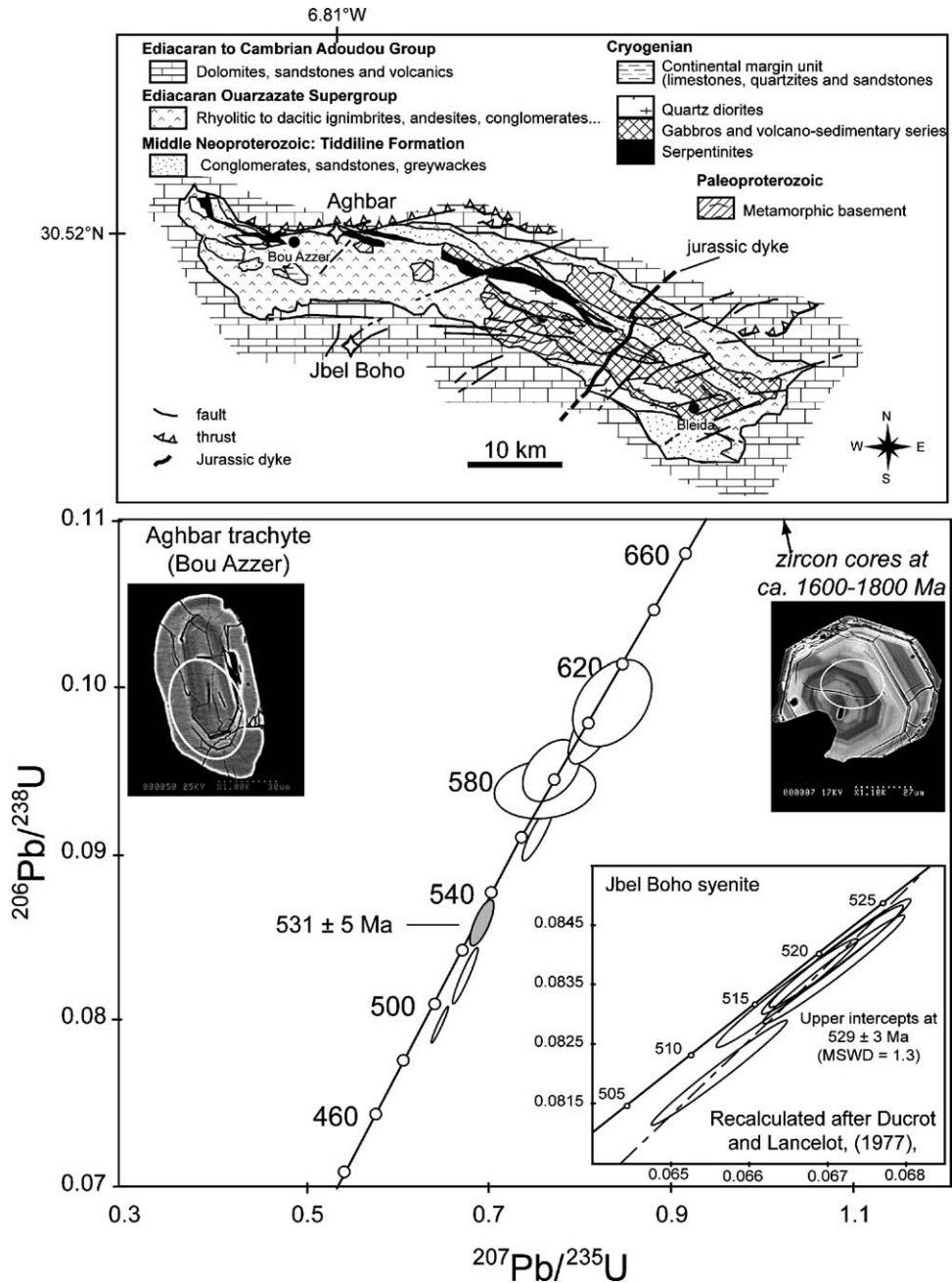
Fig. 4. Main geological units of the Bou Azzer inlier (simplified after Leblanc, 1981) and concordia diagram for zircons from the Aghbar trachyte. The $^{206}Pb/^{238}U$ age of the younger concordant point corresponds to the emplacement age of the trachyte sill (see text). Ellipses are 2σ errors. The age of the Jbel Boho syenite has been recalculated with Isoplot (Ludwig, 2003) from data of Ducrot and Lancelot (1977). Errors corresponds to the error average given by the authors; the error correlation value is 0.98. Star represents the position of the dated trachyte and syenite.

Table 1

U–Pb isotopic data (SIMS-CAMECA IMS 1270, Nancy, France) for zircon grains from the Ediacaran magmatism from the Saghro–Imiter, Ougnat–Bou Madine and Bou Azzer inliers

Sample	Measured data					Concentration (ppm)			Tera-Wasserburg Concordia data				Conventional concordia data					Ages (Ma)			
	Is^{206}Pb	$^{207}\text{Pb}/^{206}\text{Pb}$	$^{204}\text{Pb}/^{206}\text{Pb}$	$^{206}\text{Pb}/^{238}\text{U}$	UO/U	Pb	U	Th	$^{238}\text{U}/^{206}\text{Pb}$	$\pm\sigma$	$^{207}\text{Pb}/^{206}\text{Pb}$	$\pm\sigma$	$^{207}\text{Pb}/^{235}\text{U}$	Error	$^{206}\text{Pb}/^{238}\text{U}$	Error	Correlation error	$^{206}\text{Pb}/^{238}\text{U}$	Error	$^{207}\text{Pb}/^{235}\text{U}$	Error
BM7 (Ougnat–Bou Madine, rhyolite, limpid grains)																					
12–18	4531	0.0644	0.00035	0.208	7.51	32	425	174	11.2938	0.1526	0.0644	0.0003	0.7356	0.0116	0.0885	0.0012	0.859	547	7	560	7
38–14	3837	0.0648	0.00059	0.204	7.44	36	472	223	11.2687	0.2268	0.0648	0.0024	0.7020	0.0360	0.0887	0.393	548	11	540	21	
3–15	11314	0.1099	0.00361	0.127	7.77	80	1975	1099	21.3385	0.4168	0.1099	0.0006	0.3738	0.0117	0.0469	0.0009	0.623	295	6	322	9
40-3	5639	0.0603	0.00011	0.219	7.74	41	548	238	11.4911	0.1560	0.0603	0.0002	0.7131	0.0107	0.0870	0.0012	0.902	538	7	547	6
43-8	7893	0.0865	0.00187	0.175	7.55	62	1009	787	13.9941	0.2939	0.0865	0.0031	0.5909	0.0457	0.0715	0.0015	0.272	445	9	471	29
43-9	2070	0.0734	0.00135	0.184	7.10	25	322	123	11.1924	0.3062	0.0734	0.0008	0.6858	0.0349	0.0893	0.0024	0.538	552	14	530	21
44-4	5489	0.0591	0.00002	0.235	7.83	40	517	177	10.9875	0.1559	0.0591	0.0002	0.7475	0.0111	0.0910	0.0013	0.952	562	8	567	6
4-10	5948	0.0656	0.00041	0.214	7.64	50	662	266	11.4408	0.1538	0.0656	0.0003	0.7272	0.0132	0.0874	0.0012	0.743	540	7	555	8
4-7	6803	0.0754	0.00113	0.246	8.03	50	656	234	11.3496	0.1665	0.0754	0.0004	0.7244	0.0167	0.0881	0.0013	0.637	544	8	553	10
7-1	26581	0.0681	0.00063	0.380	9.41	62	850	356	11.8578	0.1007	0.0681	0.0003	0.6870	0.0088	0.0843	0.0007	0.665	522	4	531	5
7-12	11053	0.0660	0.00045	0.410	9.91	27	384	112	12.1114	0.0678	0.0660	0.0002	0.6793	0.0056	0.0826	0.0005	0.678	511	3	526	3
7-16	30385	0.0670	0.00038	0.400	9.48	63	834	320	11.3788	0.0846	0.0670	0.0008	0.7475	0.0413	0.0879	0.0007	0.389	543	4	567	8
7-19	19993	0.0599	0.00004	0.430	9.59	49	610	285	10.7606	0.0746	0.0599	0.0001	0.7629	0.0057	0.0929	0.0006	0.931	573	4	576	3
7-20	9929	0.0595	0.00004	0.450	9.98	24	315	174	11.0989	0.0705	0.0595	0.0003	0.7350	0.0057	0.0901	0.0006	0.814	556	3	559	3
7-21	12822	0.0604	0.00010	0.480	10.35	33	428	123	11.1435	0.0761	0.0604	0.0001	0.7328	0.0052	0.0897	0.0006	0.971	554	4	558	3
7-25	13215	0.0644	0.00038	0.450	9.84	32	399	166	10.8728	0.1277	0.0644	0.0004	0.7495	0.0109	0.0920	0.0011	0.809	567	6	568	6
7-3	17284	0.0595	0.00002	0.450	9.84	39	486	186	10.8019	0.0586	0.0595	0.0001	0.7587	0.0043	0.0926	0.0005	0.965	571	3	573	2
7-4	17866	0.0592	0.00001	0.420	9.59	43	551	239	11.0108	0.0622	0.0592	0.0001	0.7422	0.0043	0.0908	0.0005	0.981	560	3	564	2
BM7 (Ougnat–Bou Madine, rhyolite, inherited core)																					
7-2	9175	0.1800	0.00054	1.980	9.84	21	62	39	2.4780	0.0220	0.1800	0.0004	9.6636	0.0971	0.4035	0.0036	0.882	2185	16	2403	9
IM74 (Saghro–Imiter, Tachkakacht rhyolite, limpid grains)																					
74-1	29146	0.1896	0.00920	0.566	10.08	59	797	196	11.5425	0.1204	0.1896	0.0018	0.6654	0.0450	0.0866	0.0009	0.154	536	5	518	27
74-10	108462	0.2527	0.00108	0.552	11.01	245	3333	2540	11.6809	0.0965	0.2527	0.0034	2.8428	0.0485	0.0856	0.0007	0.484	530	4	1367	13
74-11	23921	0.0786	0.00138	0.510	10.30	52	694	148	11.3672	0.0968	0.0786	0.0013	0.7132	0.0259	0.0880	0.0007	0.235	544	4	547	15
74-12	79577	0.1716	0.00802	0.508	9.54	219	2887	1216	11.3506	0.0997	0.1716	0.0006	0.6647	0.0174	0.0881	0.0008	0.335	544	5	517	11
74-13	15705	0.0873	0.00192	0.523	10.35	38	505	126	11.2928	0.0766	0.0873	0.0009	0.7296	0.0191	0.0886	0.0006	0.259	547	4	556	11
74-14	33336	0.0604	0.00010	0.500	10.14	104	1332	341	11.0171	0.0626	0.0604	0.0001	0.7393	0.0044	0.0908	0.0005	0.957	560	3	562	3
74-15	71200	0.0766	0.00132	0.455	9.84	210	2876	1126	11.7491	0.0986	0.0766	0.0004	0.6744	0.0095	0.0851	0.0007	0.596	527	4	523	6
74-17	7509	0.1247	0.00452	0.736	11.76	41	492	88	10.4086	0.1085	0.1247	0.0015	0.7885	0.0402	0.0961	0.0010	0.205	591	6	590	23
74-3	91970	0.1057	0.00327	0.481	10.16	202	2861	959	12.1917	0.1282	0.1057	0.0039	0.6598	0.0749	0.0820	0.0009	0.093	508	5	514	45
74-5	39739	0.0604	0.00011	0.505	10.11	96	1217	362	10.8683	0.0656	0.0604	0.0002	0.7475	0.0063	0.0920	0.0006	0.714	567	3	567	4
BA06 (Bou Azzer, Aghbar trachyte, limpid grains)																					
6-1	19113	0.0626	0.00018	0.490	10.51	61	779	195	10.9699	0.1355	0.0626	0.0002	0.7553	0.0103	0.0912	0.0011	0.904	562	7	571	6
6-11a	26251	0.0677	0.00061	0.460	10.17	79	972	451	10.5442	0.1338	0.0677	0.0009	0.7705	0.0212	0.0948	0.0012	0.460	584	7	580	12
6-11b	24248	0.0720	0.00089	0.460	10.19	74	924	406	10.6724	0.1324	0.0720	0.0018	0.7634	0.0368	0.0937	0.0012	0.257	577	7	576	21
6-15	12454	0.0620	0.00019	0.670	12.16	56	795	129	12.1024	0.1549	0.0620	0.0003	0.6761	0.0093	0.0826	0.0011	0.927	512	6	524	6
6-2	16074	0.0594	0.00003	0.400	10.3	49	720	149	12.5365	0.1219	0.0594	0.0001	0.6485	0.0064	0.0798	0.0008	0.979	495	5	508	4
6-4a	9940	0.0639	0.00021	0.550	10.64	30	351	120	10.1710	0.2004	0.0639	0.0007	0.8255	0.0227	0.0983	0.0019	0.715	605	11	611	13
6-4b	10041	0.0671	0.00040	0.550	10.61	30	351	119	10.1148	0.1602	0.0671	0.0014	0.8370	0.0303	0.0989	0.0016	0.437	608	9	618	17
6-9	1758	0.1400	0.00503	0.580	10.56	6	76	37	10.3185	0.2223	0.1400	0.0034	0.9071	0.0818	0.0969	0.0021	0.239	596	12	655	43
BA06 (Bou Azzer, Aghbar trachyte, inherited grains)																					
6-12	1808	0.1100	0.00011	1.950	10.96	6	21	11	3.1350	0.0457	0.1100	0.0003	4.7745	0.0733	0.3190	0.0047	0.951	1785	23	1780	13
6-14	19449	0.1200	0.00033	2.030	12.18	104	488	12	4.0211	0.1036	0.1200	0.0010	3.9660	0.1091	0.2487	0.0064	0.937	1432	33	1627	22

A CAMECA IMS 1270 ion microprobe (CRPG-CNRS, Nancy, France) was used following the analytical methods described in Deloule et al. (2002). Detailed optical microscope and SEM–BSE investigations revealed the structures of the 50–150 μm zircon grains. The data are presented in Table 1 and discussed below. Weighted mean ages and concordia diagrams were plotted using the Isoplot program (Ludwig, 2003).

4.2. Ougnat–Bou Madine

One sample from the rhyolitic dome of the Bou Madine mine was dated. The zircons are limpid, euhedral, bipyramidal crystals with well-developed 50–150 μm prisms. They contain occasional primary cracks and inclusions (apatite, monazite, quartz, rare micas and K-feldspars) and display a thin oscillatory zoning of magmatic origin and rare inherited cores.

Eleven sub-concordant points gave a weighted mean age of 552 ± 5 Ma (Fig. 2). This age is interpreted as the crystallisation age of the rhyolitic dome of the Ougnat inlier. It thus represents a minimum age for the Ediacaran felsic volcanism. A zircon core yielded a Palæoproterozoic age (>2100 Ma) suggesting that the core may be an inherited xenocryst from a significantly older underlying basement.

4.3. Saghro–Imiter

The Tachkakacht rhyolitic dyke contains small (<80 μm) limpid zircons. They are euhedral and bipyramidal with well-developed prisms. Primary cracks and inclusions (apatite, quartz, occasional micas) are rare. Oscillatory zoning of magmatic origin is seen infrequently and none of the grains had inherited cores.

Seven sub-concordant points gave a weighted mean age of 543 ± 9 Ma (Fig. 3). This is in good agreement with the 550 ± 3 Ma age of the neighbouring Takhatert rhyolitic dome and with the stratigraphic position of the felsic volcanism, which belongs to the Edicaran Ouarzazate Supergroup. Three other zircons yielded concordant ages of between 560 and 600 Ma. They probably represent xenocrysts inherited from granitoids and Ediacaran volcanic rocks. Their ages are in accordance with the inherited ages obtained by Cheilletz et al. (2002) from the Takhatert rhyolitic dome.

4.4. Bou Azzer–Aghbar

One sample of the Aghbar trachytic sill was analyzed. The zircons are limpid and sub-euhedral, with very small prisms (50–80 μm). They contain rare inclusions of apatite, quartz and micas and show oscillatory zoning of magmatic origin and rare inherited cores.

Six very small (50–60 μm) zircon grains are scattered along the concordia between 560 and 615 Ma. They are probably inherited zircons from the basement country rocks. The youngest concordant zircon gives an age of 531 ± 5 Ma (Fig. 4). This age is in agreement with the stratigraphic position of the sill, which was intruded into an early Cambrian series (Choubert, 1952; Leblanc, 1981), and with the 529 ± 3 Ma age of the Jbel Boho syenite (Fig. 4) (recalculated from Ducrot and Lancelot, 1977). Two zircons gave Statherian ages (ca. 1600–1800 Ma; Table 1). They probably represent xenocrysts inherited from the underlying Palæoproterozoic basement.

5. Geochemistry of the Ediacaran and Cambrian magmatism in the AA area

The geochemical characteristics of the Ediacaran (Ouarzazate Supergroup) and Cambrian (Taroudant Group) post-orogenic magmatism were determined using previously published U–Pb data for the whole AA, together with analyses from the Saghro–Imiter, Ougnat–Bou Madine and Bou Azzer inliers (Figs. 5–7; Tables 2 and 3).

5.1. Major and trace elements

(i) The 595–570 Ma magmatism is represented by kilometer-scale intrusive bodies of granites, granodiorites and tonalities, with minor diorites and gabbros, and rare basalts and andesites. All rock types show mostly metaluminous (50% < SiO_2 < 75%), high-K calc-alkaline affinities (Fig. 5a). Na_2O/K_2O ratios range from 0.28 to 4.67, REE patterns (Fig. 6a) are moderately fractionated [6.43 < $(La/Yb)_N$ < 27.63] with relatively low Yb_N contents (≤10) and low nega-

Table 2

Representative major (wt.%) and trace (ppm) element analyses from Saghro–Imiter inlier

Sample type	B. Madine	Imiter								B. Azzer
	BM99-01 rhyolite	SJ127 granite	IM99-50 granite	IM00-03 diorite	IM99-72 rhyolite	IM99-05 rhyolite	IM99-74 rhyolite	IM99-75 ignimbrite	IM01-01 rhyolite	BA99-6 trachyte
SiO_2	77.06	66.28	68.72	55.17	73.26	72.66	77.30	75.51	76.29	64.33
Al_2O_3	12.33	15.45	14.53	17.14	13.53	13.56	11.99	12.98	12.51	13.87
Fe_2O_3	0.83	4.00	3.10	8.36	2.31	1.80	1.13	1.36	1.26	7.63
MnO	0.10	0.08	0.08	0.14	0.07	<DL	<DL	<DL	<DL	<DL
MgO	0.27	2.01	1.50	4.82	0.84	0.31	0.22	0.23	0.18	1.34
CaO	0.32	1.06	1.40	6.33	0.63	0.36	0.21	0.42	0.26	1.43
Na_2O	1.22	3.38	3.13	2.88	2.80	1.85	2.79	4.17	3.88	2.09
K_2O	5.87	4.40	3.91	2.31	4.67	8.05	5.63	4.33	4.66	5.98
TiO_2	0.12	0.48	0.17	0.85	0.18	0.07	0.06	0.05	0.09	0.45
P_2O_5	<DL	0.16	0.11	0.19	0.02	0.03	<DL	<DL	0.06	<DL
LOI	1.77	2.68	3.20	1.71	1.61	1.20	0.63	0.77	0.76	2.69
Total	99.89	99.98	99.85	99.90	99.92	99.92	99.96	99.82	99.95	99.81
As	15	341	58	7	36	2.30	15	3	25	15
Ba	1325	1560	747	618	466	1388	1677	1178	1847	369
Cr	10	42	7	121	13	0.3	<DL	<DL	<DL	<DL
Cu	111	10	6	41	27	5.6	15	<DL	10	<DL
Hf	6.0	3.9	2.9	2.8	5.0	3.4	2.9	3.1	4.0	16.3
Mo	3.3	1.9	0.9	1.0	1.5	1.1	3.6	<DL	2.0	3.1
Nb	11.4	6.3	5.9	4.6	13.4	7.8	7.2	7.0	8.2	115
Ni	<DL	12	5	24	3	2	<DL	<DL	<DL	<DL
Pb	95	90	47	6	239	11	77	6	133	5
Rb	149	139	108	85	150	195	139	124	120	114
Sr	50	362	109	466	75	58	77	89	105	29
Th	13.0	8.6	6.6	4.3	12.4	12	11.7	10.9	10.4	17.0
U	4.3	4.8	2.9	2.4	5.1	4	5.0	6.6	5.4	3.2
V	5	65	14	159	17	3	2	3	2	2
Y	35.1	12.7	7.4	16.2	26.5	18.4	15.4	10.3	21.6	73.3
Zn	284	153	75	100	901	18	21	27	58	15
Zr	203	137	110	103	147	109	86	87	131	703
La	37.7	25.5	19.7	15.1	33.3	36.1	25.6	25.3	43.6	102.0
Ce	85.5	50.0	36.3	30.6	62.4	71.2	49.2	47.1	83.0	208.0
Pr	9.5	5.5	4.2	3.6	7.8	7.1	5.3	5.0	8.8	24.0
Nd	37.0	20.8	16.2	14.0	29.6	23.8	18.5	17.0	32.3	88.1
Sm	6.5	3.9	3.0	3.1	6.0	4.1	3.1	2.7	5.4	16.2
Eu	0.8	1.0	0.7	1.0	0.5	0.8	0.5	0.4	0.7	2.4
Gd	5.8	2.8	2.4	3.0	4.8	2.7	2.2	2.1	4.4	12.6
Tb	0.9	0.4	0.3	0.4	0.7	0.4	0.4	0.3	0.6	2.0
Dy	5.3	2.5	1.5	2.6	4.5	2.6	2.3	1.8	3.4	12.2
Ho	1.0	0.5	0.2	0.5	0.9	5.0	0.5	0.3	0.7	2.6
Er	2.9	1.3	0.6	1.4	2.5	1.6	1.4	1.0	1.9	7.2
Tm	0.4	0.2	0.1	0.2	0.4	0.3	0.2	0.2	0.3	1.0
Yb	2.9	1.3	0.5	1.6	2.6	1.8	1.6	1.0	2.1	6.8
Lu	0.5	0.2	0.1	0.3	0.4	0.3	0.2	0.2	0.4	1.0

Analytical methods: Major element concentrations were determined by ICP-AES, and trace elements by ICP-MS at CRPG-CNRS (Nancy, France). Analytical uncertainties are estimated at 2% for major elements, and at 5 or 10% for trace-element concentrations (except REE) higher or lower than 20 ppm, respectively. Precision for REE is estimated at 5% when chondrite-normalized concentrations are >10 and at 10% when they are lower. $Fe_2O_3{}^*$: total iron; <DL: below detection limit; LOI: loss on ignition.

Table 3

Available Sr and Nd isotopic compositions of (595–570 Ma) granite-granodiorites and (570–545 Ma) rhyolites from the Imiter Inlier

Age/sample	Type	Sr (ppm)	Rb (ppm)	$^{87}Rb/^{86}Sr$	$^{87}Sr/^{86}Sr$ ($\pm 2\sigma$)	$(^{87}Sr/^{86}Sr)t$
Rb-Sr data						
595–570 Ma						
IM 99-50	Granodiorite	115.22	106.7	2.68	0.724462 (24)	0.7034
IM 00-03	Granodiorite	482.48	101.0	0.61	0.710785 (24)	0.7060
SJ 127	Granite	349.57	125.5	1.04	0.714448 (16)	0.7063
570–545 Ma						
IM 99-72	Rhyolite	103.98	113.5	3.16	0.729262 (22)	0.7045
IM 99-74	Rhyolite	73.01	133.3	5.30	0.744363 (18)	0.7028
IM 99-75	Ignimb. rhyolite	87.05	120.3	4.01	0.733671 (15)	0.7023
IM 01-01	Rhyolite	101.96	112.8	3.23	0.729407 (21)	0.7041

Age/sample	Sm (ppm)	Nd (ppm)	$^{147}Sm/^{144}Nd$	$^{143}Nd/^{144}Nd$ ($\pm 2\sigma$)	$^{143}Nd/^{144}Ndt$	ε_{Ndt}	T_{DM} (Ma)
Sm-Nd data							
595–570 Ma							
IM 99-50	3.26	16.8	0.1172	0.512059 (11)	0.511615	−11.15	1462
IM 00-03	3.42	16.8	0.1228	0.512220 (21)	0.511687	−8.00	1561
SJ 127	3.39	19.4	0.1059	0.512188 (11)	0.511737	−8.61	1305
570–545 Ma							
IM 99-72	4.55	27.4	0.1005	0.512267 (15)	0.511789	−7.07	1275
IM 99-74	3.38	18.4	0.1110	0.512096 (9)	0.511701	−10.41	1269
IM 99-75	2.75	18.0	0.0922	0.512158 (25)	0.511775	−9.21	1161
IM 01-01	5.05	30.1	0.1015	0.512197 (18)	0.511798	−8.45	1152

Analytical method: Separation of Rb–Sr and Sm–Nd was made according to the methods of Michard et al. (1985) and Boher et al. (1992). Rb, Sr, Sm and Nd concentrations were determined by isotope dilution. Rb was analyzed by thermal ionisation on a Cameca TSN-206SA mass spectrometer. Sr and Nd isotopic ratios and Sm concentration were measured using a Finnigan MAT-262 mass spectrometer. Measured $^{87}Sr/^{86}Sr$ and $^{143}Nd/^{144}Nd$ ratios were normalized to $^{86}Sr/^{88}Sr = 0.1194$ and $^{146}Nd/^{144}Nd = 0.7219$, respectively. Repeated analyses of standards NBS-987 for Sr and JM for Nd gave average ratios of $^{87}Sr/^{86}Sr = 0.710205 \pm 23$ (2σ) and $^{143}Nd/^{144}Nd = 0.511095 \pm 16$ (2σ). The blanks for Sr and Nd are negligible (<2 ng for Sr and 0.4 ng for Nd) compared to the extracted quantities from samples. Analytical errors on isotopic ratios (error in the last two digits of the Sr and Nd isotopic ratios) are expressed as 2σ (= 2 standard errors of the mean). Nd model ages are calculated according to the depleted mantle model of Ben Othman et al. (1984).

tive Eu anomalies ($0.75 < Eu/Eu^* < 1.03$). They mostly belong to a high-K calc-alkaline magmatic series (Le Maitre et al., 1989), or to an alkali-calcic metaluminous (Frost et al., 2001) series.

(ii) The 570–545 Ma magmatism is represented by thick (up to 2 km near Ouarzazate) rhyolitic-ignimbritic lava flows or domes (domes, shallow intrusions) and dykes, which are mainly at the top of the sequence, with andesitic flows and rare basalts at the bottom (Bajja, 2001; Chalot-Prat et al., 2001). Alteration (sericitisation, carbonatation, hematisation, albitisation, chloritisation) of these rocks by hydrothermal fluids is common. Unaltered rock types have Na_2O/K_2O ratios >2.04, moderately fractionated REE patterns ($1.32 < La/Yb_N < 16.68$) and stronger negative Eu anomalies for the rhyolites ($0.24 < Eu/Eu^* < 0.59$) than for the andesites ($0.56 < Eu/Eu^* < 0.77$) and basalts ($0.67 < Eu/Eu^* < 1.06$). They belong to high-K calc-alkaline to shoshonitic series.

(iii) The 530 Ma magmatism consists of a trachyte sill (Aghbar) and syenite volcano (Jbel Boho; Ducrot and Lancelot, 1977) in the central AA (Bou Azzer area). The Aghbar trachyte has a high $Na_2O + K_2O$ content (8.07%), a Na_2O/K_2O ratio of 0.35, a moderately fractionated REE pattern ($La/Yb_N = 10.2$) with a negative Eu anomaly (Eu/Eu^* 0.51) and a high REE content ($\sum REE = 1700$ ppm). This magmatism belongs to a typical alkaline-shoshonitic series.
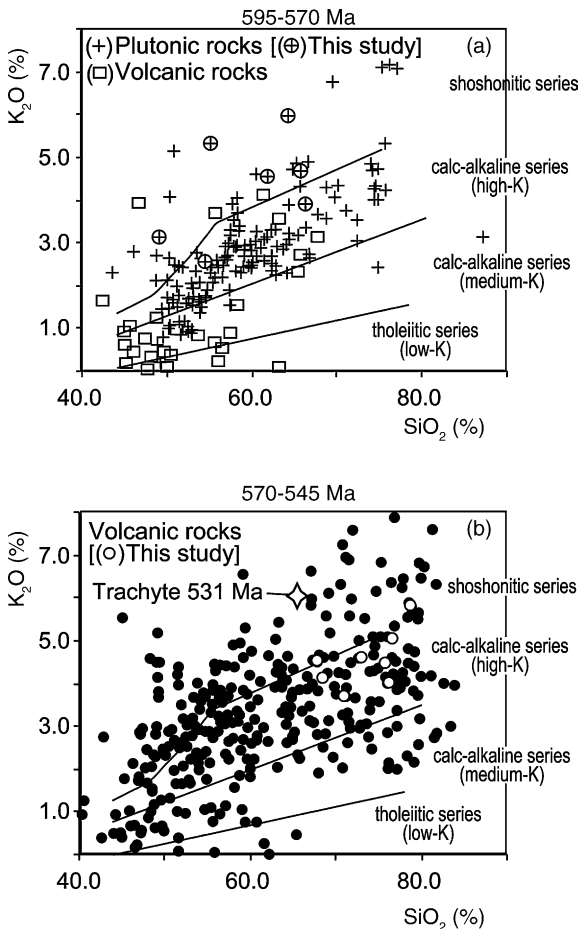
Fig. 5. K_2O–SiO_2 plots (Le Maitre et al., 1989) of selected Ediacaran calc-alkaline to alkaline plutonic (a) and volcanic (b) rocks and of the Cambrian Aghbar trachytic sill (star) of the Anti-Atlas belt. Unaltered (LOI < 3%) rocks are from this study and from Lebrun (1982), Freton (1988), Ighid et al. (1989), Azizi Samir et al. (1990), Aït Saadi (1992), Camara (1993), Mokhtari (1993), Aït Isha (1996), Aït Malek (1997), Ouguir (1997), Ikenne (1997), Eddif et al. (2000), Thomas et al. (2000), Bajja (2001), Barbey et al. (2001), Chalot-Prat et al. (2001), Gasquet et al. (2001), Karl et al. (2001), Levresse (2001), Ouazzani et al. (2001) and Thomas et al. (2002).

5.2. Isotope geochemistry

5.2.1. Rb–Sr, Sm–Nd, S and rare gas

Sr–Nd isotopic data for the 595–570 Ma plutonic event and 570–545 Ma volcanic episode in the Saghro–Imiter district are presented in Table 3 and Fig. 7. The two groups display the same low $^{87}Sr/^{86}Sr$ (0.702–0.706) and $^{143}Nd/^{144}Nd$ (0.5116–0.5119) ini-

tial ratios, which attest to a mixing of mantle and lower crustal sources, based on the mean geochemical characteristics of these reservoirs as determined by Faure (2001). The calculated Nd model ages for the 595–570 Ma granites and 570–545 Ma felsic volcanics (Table 3) fall within the rather restricted range of 1161–1561 Ma. No Mesoproterozoic rocks have been found in the AA, so it seems probable that these T_{DM} ages are the result of the mixing of an older 2 Ga source with a younger Neoproterozoic one.

The $\delta^{34}S_{CDT}$ values for the silver mineralisation event indicate preferential degassing of SO_2 in ascending fluids, as well as mixing between the magmatic isotopic reservoir and the country rock reservoir (Levresse et al., 2004). Helium isotope analyses of sulphides and gangue minerals yield similar results, with $^3He/^4He$ ratios ranging from 0.76 to 2.64R_a. These data, together with the absence of ^{20}Ne in the analyzed fluid inclusions, suggest a mantle origin for the fluids associated with the epithermal silver event (Levresse et al., 2004).

5.2.2. Re–Os

The sulphide phases and Ag^0 minerals show measured $^{187}Os/^{188}Os$ ratios of 0.144–0.197, clearly indicating a dominantly mantle source for the osmium and, by inference, the silver (Levresse et al., 2004). In order to assess the validity of this Re–Os isotope data based interpretation of the source of the metals at Imiter, we have compared our data with the Re–Os geochemical signatures of a variety of precious metal deposits from around the world, formed under different geodynamic regimes and at different times (Table 4). The measured $^{187}Os/^{188}Os$ of the Imiter epithermal deposit (0.144–0.197) is similar to the Chinkuashih Au–Cu epithermal deposit (0.13–0.24; Shen and Yang, 2004). Other gold bearing epithermal and porphyry-type deposits show a larger range of measured $^{187}Os/^{188}Os$ ratios (0.21–90.2), indicating the degree to which the primitive magma was contaminated by crustal and/or host country rocks (mean mantle: 0.12–0.13; Chen et al., 1998; mean continental crust: 1.2–1.3; Esser and Turekian, 1993). The results obtained for the Imiter Re–Os isotope system concur with the data from other geochemical proxies (see above). They are also consistent with the low initial $^{187}Os/^{188}Os$ ratios (0.28–0.62) obtained on pyrites from the 545 Ma volcanics and their relatively primitive Sr signatures, reinforcing the probable genetic link

Table 4
Re–Os isotopic compositions of the Epithermal Ag–Hg Imiter deposit and a variety of precious metal deposits in the world formed in various geodynamic setting and different epochs

| Type of deposit	Localization	[Re]	[Os]	$^{187}Re/^{188}Os$	$^{187}Os/^{188}Os$	$^{187}Os/^{188}Os(i)$	Age	Reference
Epithermal-Ag	Imiter, Morocco	0–0.06 ppb	0.006–0.162 ppb	0–14.2	0.144–0.197	0.013–0.197	Late Proterozoic	Levresse et al. (2004)
Epithermal-Au	Low-sulphidation, Bucaramanga, Colombia	43–153 ppb	21–30 ppt	244–1299	1.51–8.48	–	Paleocene	Mathur et al. (2003)
	High sulphidation, Bucaramanga, Colombia	0.8–33 ppb	19–34 ppt	8651–56136	1.85–8.11	1.2	Paleocene	Mathur et al. (2003)
	Au–Cu, Chinkuashih, Taiwan	1.4–2.9 ppb	0.2–2.1 ppb	3.7–34.5	0.13–0.24	1.15–2.07	Pliocene	Shen and Yang (2004)
Gold shear-zone	Kimberley, Zimbabwe	314–2378 ppt	28.4–88 ppt	50.4–456.5	2.01–4.83	2	Late Archean	Frei et al. (1998)
Porphyry	Base-metal PC, large, Chile	0.3–320 ppb	4–244 ppt	96-94730	0.21–78.46	0.155–1.23	Eocene	Mathur et al. (2000a,b)
	Base-metal PC, small, Chile	0.8–464 ppb	6–32 ppt	1202–120921	4.3–90.2	3.8–4.68	Eocene	Mathur et al. (2000a,b)
	Cu–Mo PC, Bagdad-vein 1, USA	3.86–6.76 ppt	8–17 ppt	2.4–19.9	5.1–32.1	2.12	Maastrichtian	Barra et al. (2003)
	Cu–Mo PC, Bagadad-vein 2, USA	1.68–4.1 ppt	6–12 ppt	1–914	1.06–10.8	0.13–0.83	Maastrichtian	Barra et al. (2003)
	Cu–Au PC stage 2, Grasberg, Irian Jaya	11–140 ppb	32–1024 ppt	751–5653	1.03–1.31	0.79–1.26	Pliocene	Mathur et al. (2000a, 2000b)
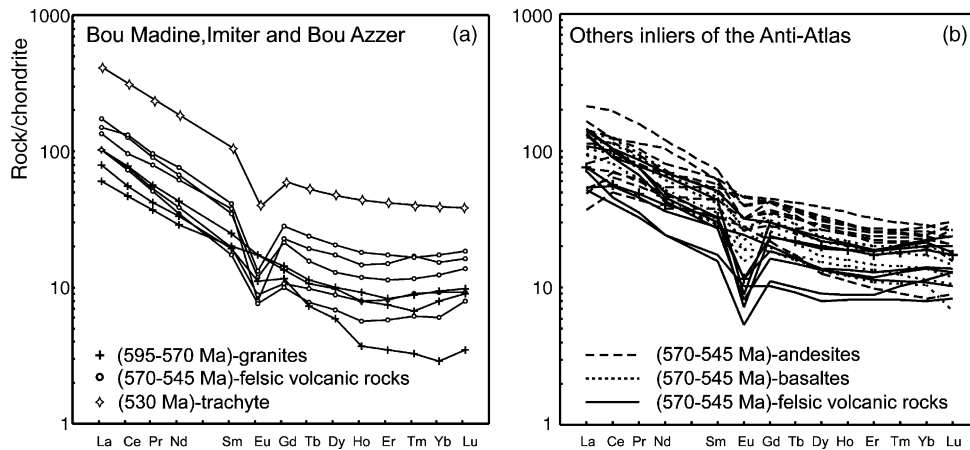
Fig. 6. Chondrite-normalized REE patterns of the Ediacaran and Cambrian plutonic and volcanic rocks from the Saghro–Imiter and Bou Azzer area (a, this study) and from the Central and Eastern Anti-Atlas (b), after Bajja (2001) and Chalot-Prat et al. (2001). Normalization values from Evensen et al. (1978).
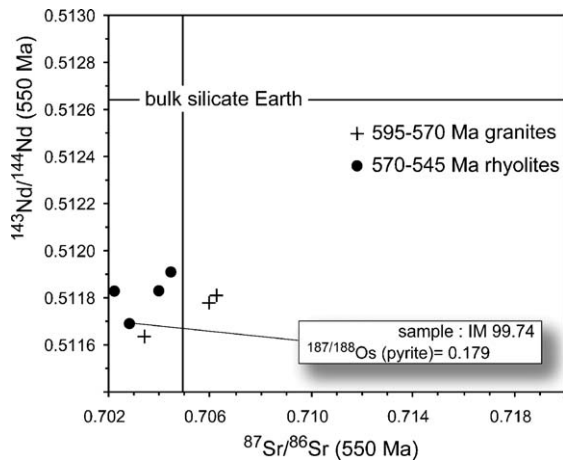

Fig. 7. $^{87}Sr/^{86}Sr$ vs $^{143}Nd/^{144}Nd$ plot of late granites and rhyolites from the Saghro–Imiter area. The mantellic initial (550 Ma) $^{187}Os/^{188}Os$ signature of euhedral pyrite of rhyolitic intrusion from Saghro–Imiter (Levresse et al., 2004) is also shown.

between this volcanic event and the epithermal silver mineralisation.

The geochemical characteristics of the Imiter deposit appear to be dominated by metals and fluids of mostly mantle origin. This result, and the huge concentration of silver at Imiter (more than 8000 metric tonnes), is consistent with observations made on Chilean base–metal porphyry deposits (Table 4), where a direct relationship between the volume of total metal concentration and the participation of a mantle source has been elucidated (Mathur et al., 2000a,b). This also demonstrates the need to invoke a major extensional tectonic regime at the time of the Imiter mineralizing event (570–545 Ma) to account for the rapid transfer of a relatively large quantity of metals directly from the mantle to the surface. The geochemical characterisation of other precious metal deposits in the AA belt is currently in progress.

6. Discussion

6.1. Synthesis of the lithostratigraphic and geochronological data for the Pan-African AA

Three lithostrathigraphic columns have been drawn up for three sections of the Western, Central and East-

Fig. 8. Structural map and reliable U–Pb radiometric ages (new and previous) of the Neoproterozoic plutonic and volcanic rocks in the Anti-Atlas and a proposed timetable. Western Anti-Atlas data are from Hassenforder (1987), Aït Malek et al. (1998), Gasquet et al. (2001), Walsh et al. (2002); Central Anti-Atlas from Ducrot and Lancelot (1977), Leblanc and Lancelot (1980), Mifdal and Peucat (1985), Thomas et al. (2002), Samson et al. (2003), Inglis et al. (2004); Thomas et al. (2004); Eastern Anti-Atlas from Magaritz et al. (1991), Landing et al. (1998), Levresse (2001), Cheilletz et al. (2002). International stratigraphic ages (left, in red) are after Amthor et al. (2003) and Gradstein et al. (2004). In bold the three studied inliers.
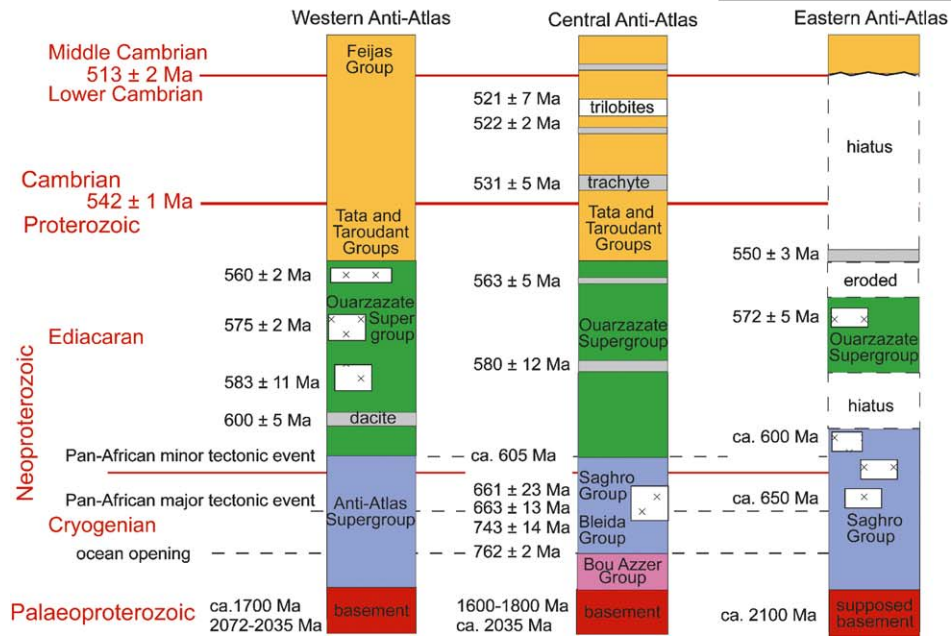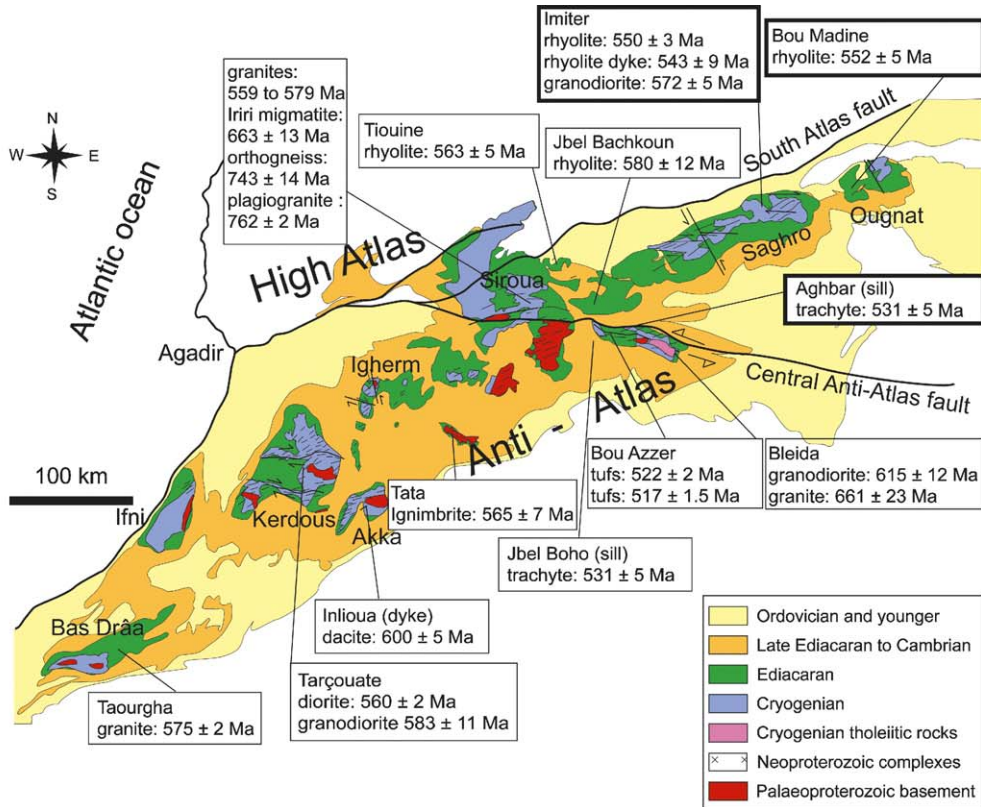
ern AA (Fig. 8). The lithostratigraphic subdivisions are based on the latest results obtained by the Moroccan National Geological Mapping Project and other recent contributions (Thomas et al., 2002, 2004; Walsh et al., 2002; Bouougri and Saquaque, 2004; Gasquet et al., 2004). By combining all this geochronological data we have been able to produce a relatively homogenous and more complete lithostrathigraphic synthesis of the AA belt.

The main points are: (i) Uniformity in the distribution of the four major units from the Palæoproterozoic basement to the Middle Cambrian sedimentary platform series. (ii) A crystalline Palæoproterozoic basement underlying the entire AA region, which supports Ennih and Liégeois's (2001) proposition that the old division of the AA into two distinct parts separated by the Central AA fault – as advocated by Choubert (1963) – be abandoned. (iii) A marked heterogeneity of Cryogenian to Ediacaran rock sequences that reflects their probable distinct origins and suggests the presence of a collage of exotic terranes (the "Anti-Atlas terranes", AAT) during the main Pan-African tectonic events. (iv) A transition, dated at 580 Ma, from a Cryogenian/early Ediacaran orogenic series to an Ediacaran post-orogenic series and finally to a Cambrian anorogenic series. (v) A voluminous (up to 2 km thick) Ediacaran volcanic sequence (upper Ouarzazate Supergroup), deposited over 30 Ma (Fig. 8), that covers most of the surface of the AA inliers and suggests the existence of a huge thermal anomaly at deep lithospheric levels. (vi) A rapid transition between a dominantly volcanic regime to a sedimentary marine epicontinental carbonate platform transgression at ca. 550 Ma, based on the last dated volcanic event (Benssaou and Hamoumi, 1999, 2001). The Tata and Taroudant Groups often unconformably/para-unconformably overly the edges of the different inliers, with a low-angle angular discordance. This is compatible with a progressive transgressive marine event (Benssaou and Hamoumi, 1999, 2001). No major geodynamic break exists between the upper part of the Ouarzazate Supergroup and the bottom of Tata and Taroudant Groups; both of which are coeval with an extensional tectonic event.

Two Pan-African tectonic events are recognised in the three sections of the AA. The first event, which was the larger of the two (Leblanc and Lancelot, 1980), has been indirectly dated at 661 ± 23 Ma from an asso-

ciated magmatism (Mifdal and Peucat, 1985) and at 663 ± 14 Ma from metamorphic rims on zircons from the Iriri migmatite (Thomas et al., 2002). The second, smaller event (Leblanc and Lancelot, 1980) took place before the Ouarzazate Supergroup magmatic event (ca. 580 Ma).

The AA belt from Morocco has been used to test international stratigraphic correlations related to the Precambrian/Cambrian boundary problem (Magaritz et al., 1991; Landing et al., 1998). However, for the three analyzed sections (Fig. 8), it can be seen that there is no direct correlation between the major limits of the lithostratigraphic groups, as they do not correspond to internationally recognised stratigraphic boundaries (Compston et al., 1992; Amthor et al., 2003; Gradstein et al., 2004).

6.2. Precise timing of Pan-African events in the Anti-Atlas (Figs. 9 and 10)

A tentative synthetic log of the tectonic and magmatic events that characterise the Precambrian–Palæozoic evolution of the AA is shown in Fig. 9. The geochronological information is reproduced from Fig. 8. Seven major magmatic episodes corresponding to major changes in geochemical characteristics and the tectonic environment have been clearly identified. The geodynamic evolution of the Pan-African belt is developed in Fig. 10 according to the four major stages proposed in Fig. 9. These magmatic events can be grouped into four stages.

Stage 1: Ocean opening. This stage has been clearly identified at Bou Azzer (Leblanc, 1975, 1981; Church, 1980; Admou, 2000; Fekkak et al., 2003), but it is less evident in the Sirwa massif (Leblanc, 1975; El Boukhari et al., 1991; Chabane, 1991; Thomas et al., 2002). However, the precise age of the associated tholeiitic magmatism has not been well-constrained. At Bou Azzer, the thermal metamorphism linked to the emplacement of gabbroic dykes, which is assumed to belong to the tholeiitic magmatic event, has been dated at 788 ± 8 Ma (Clauer, 1976; Leblanc and Lancelot, 1980). Thomas et al. (2002) obtained an age of 743 ± 14 Ma for a tonalite protolith from an orthogneiss of the ophiolitic sequence of the Bleida Group in the Sirwa inlier. Samson et al. (2003) dated the emplacement of a tholeiitic plagiogranite at 762 ± 2 Ma.
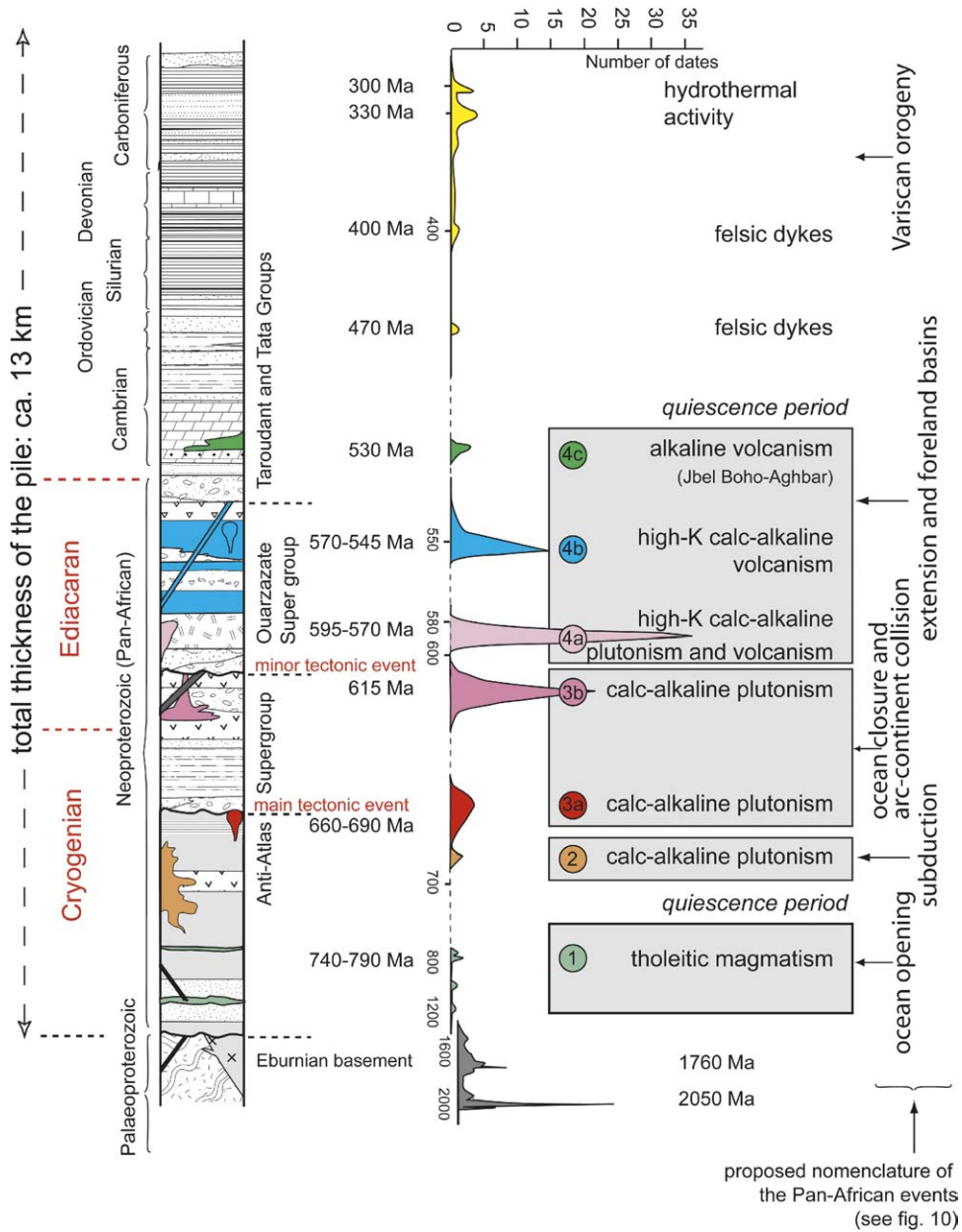
Fig. 9. Synthetic log of the Anti-Atlas series with the main tectonic events and U–Pb ages of magmatic episodes, obtained in this study or compiled from the literature: Juery (1976), Charlot (1976), Ducrot and Lancelot (1977), Ducrot (1979), Leblanc and Lancelot (1980), Mifdal and Peucat (1985), Magaritz et al. (1991), Mrini (1993), Aït Malek et al. (1998), Landing et al. (1998), Gasquet et al. (2001), Walsh et al. (2002); Cheilletz et al. (2002), Thomas et al. (2002, 2004); Barbey et al. (2004); Inglis et al. (2004). Note that the number of geochronological data is roughly proportional at the volumetric importance of the magmatisms.
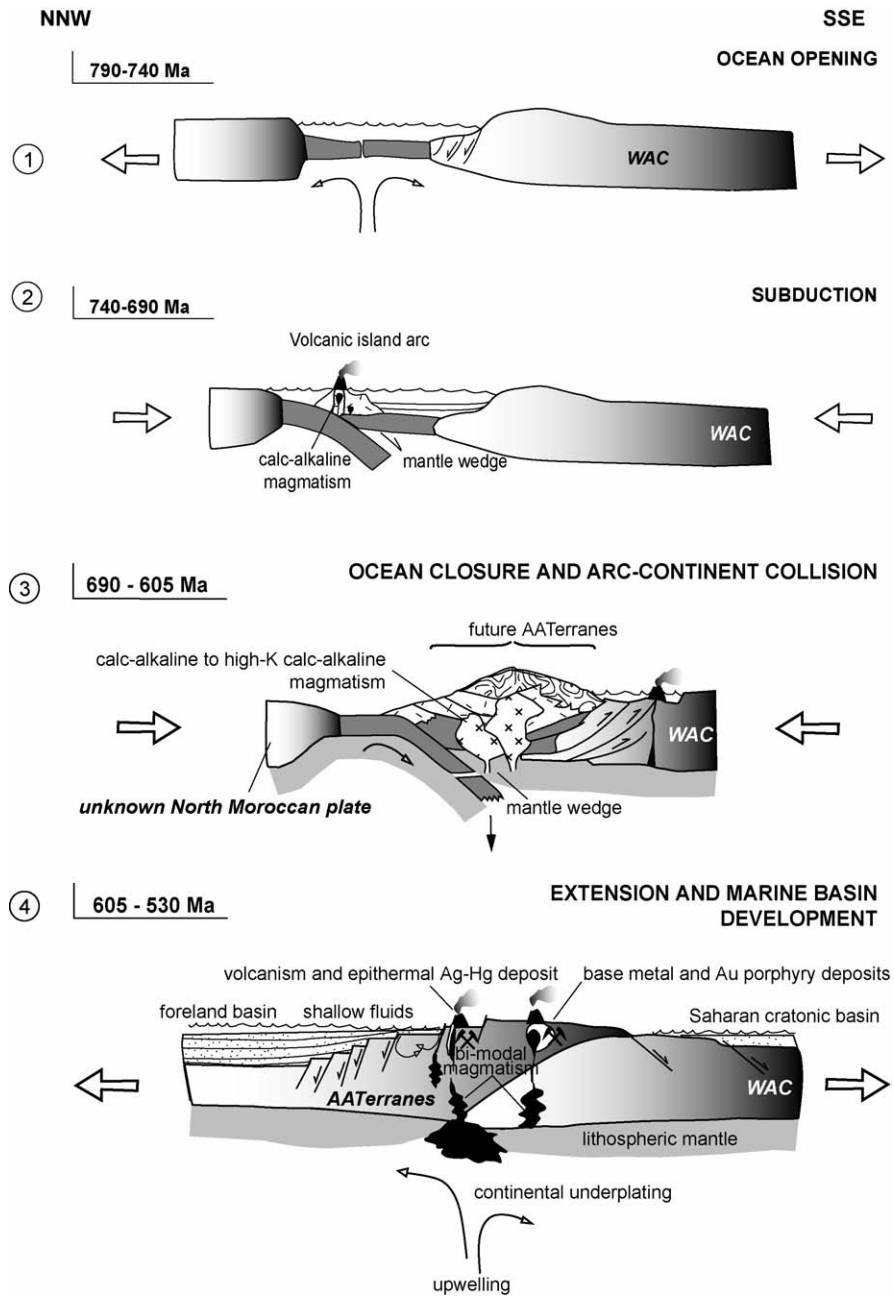
Fig. 10. Pan-African geodynamic evolution of the Anti-Atlas during Pan-African times. WAC: West African Craton, NAA: Northern Anti-Atlas (after Levresse, 2001 modified). See text.

Stage 2: Subduction. The calc-alkaline magmatism related to arc-subduction processes in Saghro and Bou Azzer has not yet been precisely dated (Saquaque et al., 1989, 1992). There is currently no consensus on whether the subduction plane dipped to the north or to the south (Leblanc, 1975; Leblanc and Lancelot, 1980; Hefferan et al., 1992; Villeneuve and Cornée, 1994; Ennih and Liégeois, 2001, 2003; Thomas et al., 2002). If viewed as an analogue to the modern western pacific margin (after Lagabrielle, in Pomerol et al., 2005), Proterozoic subduction zones in the AA might bound several microplates, so there could have been several planes with different dip directions. If this was the case in the AA belt during early Pan-African times, it would explain the conflicting interpretations and reconcile the different hypotheses. Stage 2 is also characterised by the high P-low T metamorphism of the metabasites of the Bou Azzer inlier ($T \leq 350\,^\circ$C and P of approximately 5 kbar; Hefferan et al., 2002).

Stage 3: Arc–continent collision and ocean closure:

3a. This episode was first recognised at Bou Azzer (Leblanc, 1981; Hefferan et al., 1992). It corresponds to the tectonic emplacement of the allochthonous oceanic ophiolitic slivers and is related to the main Pan-African tectonic event (660–690 Ma). Accompanying features include low-grade metamorphism, partially anatectic gneisses and calc-alkaline intrusives. The main tectonic event in the western and eastern AA has not been precisely dated, which makes correlation of this event over the whole AA difficult.

3b. This episode, which is coeval with the later, minor tectonic event, corresponds to the closure of the fore-arc and back-arc basin.

Stage 4: Extension and marine basin development:

4a. This important magmatic episode has been dated at 595–570 Ma. It is represented by intermediate to felsic (mainly high-K calc-alkaline) intrusives related to base metal ore deposits (Cu–Pb–Zn; Levresse, 2001; Cheilletz et al., 2002) and constitutes a transition towards the main Ediacaran distensive tectonic event.

4b. The Ediacaran (570–545 Ma) is characterised by a major high-K calc-alkaline to alkaline magmatism. It is intimately linked to the largest precious metal deposits (Au–Hg Imiter, Cheilletz et al., 2002)

and to base metal porphyry type mineralisations (Cheilletz and Gasquet, 2001; Abia et al., 2003). Although it has not been dated precisely, the Tiouit mesothermal Au deposit is related to high-K calc-alkaline magmatism and has been interpreted as belonging to the same event (Al Ansari and Sagon, 1997).

4c. An alkaline volcanic episode interbedded within the Cambrian platform sedimentary series at Bou Azzer–Aghbar (this work) and at Bou Azzer–Jbel Boho (Ducrot and Lancelot, 1977) has been precisely dated at 530 Ma. This alkaline volcanism is related to the general anorogenic tectonic regime to which the whole AA was subjected at this time.

The Palæozoic geodynamic cycle started after the Ediacaran–early Cambrian evolution. It is characterised by the injection of felsic dykes at 470 and 400 Ma (Huch, 1988), followed by hydrothermal activity at 330 and 300 Ma. At least part of the Au mineralisation in the Iourirn deposit (Western AA) has been recently attributed to a late Variscan event at 301 ± 7 Ma (Gasquet et al., 2004).

A total thickness of approximately 13 km of Cryogenian to Palæozoic rocks were produced and accreted along the northern border of the WAC during Pan-African times.

6.3. Inversion tectonics at the Precambrian–Cambrian boundary

AA magmatic rocks present a progressive transition from orogenic magmatic suites, episodically emplaced during the period 690–605 Ma, to high-K calc-alkaline plutonic and volcanic rocks, formed during the period 605–550 Ma, and then, 20 Ma later, to alkaline volcanism. This evolution clearly suggests a change from an orogenic to an anorogenic tectonic regime. Sedimentological and structural evidence also indicates such a transition, with the development of molasse basins controlled by extensional tectonics (Benziane et al., 1983; Chbani et al., 1999; Fekkak et al., 1999; Soulaïmani et al., 2001; Soulaimani and Piqué, 2004); the importance of normal faulting in the localisation of precious metal deposits, particularly in the epithermal Ag–Hg Imiter world-class mine (Ouguir et al., 1994; Cheilletz et al., 2002); the formation of Sedex-type early Cambrian Cu–Pb–Zn deposits (Viland, 1988; Benssaou and

Hamoumi, 1999). On the whole, the Ediacaran period in the AA strongly reflects a tectonic inversion from a compressive–transtensive regime to an extensional regime that is characteristic of the final stage of the Pan-African orogeny, resulting in a change from an active margin to a passive margin at the northern margin of the WAC. The precise structural pattern of this transition is not yet fully understood, mainly due to successive Variscan and Alpine overprints. This is particularly true for the kinematic interpretation of major faults in the AA, for example the Central AA or the South Atlas faults (Saquaque et al., 1992; Ennih and Liégeois, 2001; Oudra et al., 2003).

6.4. Geodynamic reconstruction and metallogenic activity in the Pan-African AA (Fig. 10)

It is noteworthy that the geodynamic stages and processes of the AA Pan-African belt (Fig. 10) controlled the large-scale metallogenic activity that took place in this area at the Precambrian–Lower Palæozoic boundary. Stages 1 and 2 are not developed here as they do not clearly correspond to a major metallogenic event except during the ocean opening stage 1, which is characterised in the Bleida inlier by base metal and gold mineralisations (Mouttaqi, 1997; Belkabir et al., 2004). The 690–605 Ma stage 3 corresponds to an arc–continent collision, with a moderate collision and crustal thickening. The main tectonic events were ocean floor obduction, development of a regional NE–SW schistosity, calc-alkaline to high-K calc-alkaline magmatism, and collage of meta-sedimentary and -magmatic rocks to the northern border of the WAC to form the AA Terranes (AAT). A typical active margin developed during this stage 3. However, due to a lack of precise geochronological data no specific ore deposit can be attributed to this event. The 605–530 Ma stage 4 involved the transition to a passive continental margin, coupled with extensional tectonics and the development of marine basins to the North and the Saharan cratonic basin to the South. During this period, there was a long association between magmatism and metallogenic activity (e.g. felsic volcanism and the Imiter giant Ag–Hg deposit, Cheilletz et al., 2002; Levresse et al., 2004). They have mantellic and pro parte lower continental crust signatures. Thus, a large volume of juvenile material, precious metals and chalcophile elements was added to the continental crust.

The post-collisional features, related extensive high-K calc-alkaline magmatism and marine basin development, together indicate a high heat flow contribution either due to continental underplating and/or to mantle upwelling (Kearey and Vine, 1992). This type of geodynamic environment is particularly suitable for the development of superficial hydrothermal mineralisations in the form of epithermal or base metal porphyry deposits (e.g. Cheilletz et al., 2002). Furthermore, huge metal transfers suggest the existence of vertical drains (e.g. extensional fault zones) that were able to mobilise the deepest parts of the lithosphere (Levresse et al., 2004). This model, which involves a large part of the lower crust and mantle (Kay and Mpodozis, 2001), is significantly different to the earlier re-mobilisation model for the origin of giant precious metal deposits, such as Imiter, from local superficial convective cells (Leistel and Qadrouci, 1991; Barodi et al., 1998). Thus, the Imiter silver deposit can be regarded as a Precambrian analogue to modern epithermal deposits.

7. Conclusion: the northern margin of the WAC

The evolution of the Pan-African AA belt is characterised by the successive development of extension-collision-extension events, as in all modern orogens. Here, the collision event is subdivided into two stages. However, when comparing the geodynamic evolution of the Pan-African AA belt with other Pan-African chains (Avalonia, South-America, Carolina, Hoggar, etc., for example: Murphy and Nance, 1989, 2002; Murphy, 2002; Abdesalam et al., 2002; Neves, 2003), three main differences can be noted: (i) The AA Pan-African main collisional stage (stage 3) is moderate, as revealed by the absence of large-scale crustal thickening and generalised thrusting. (ii) The AA Pan-African orogen is mostly composed of a shallow-crust terrane succession that has been subject to low-grade metamorphism. (iii) The end of the Pan-African evolution is marked by strong extensional tectonics. The metallogenic consequences of this specific orogenic belt organisation are highlighted. The most intense metallogenic activity occurred during the late extensional stage 4 at the Precambrian–Cambrian boundary. It is characterised by world-class precious metal epithermal deposits (Imiter) and base metal porphyry- and Sedex-type occurrences (Bou Madine; western AA early Cam-

brian mineralisations). It is noteworthy that orogenic gold mineralisations are lacking in the Pan-African AA belt. This might be related to the moderate crustal thickening that took place during this orogeny, which did not permit the installation of large-scale hydrothermal cells and related gold re-mobilisations.

The tectonic evolution of the AA belt can be examined on the scale of the WAC. As clearly reported by Villeneuve and Cornée (1994), during Pan-African times the western and eastern margins of the WAC were subject to completely different tectonic regimes and consequently exhibited very different behaviours The eastern margin was subject to a compressive regime; the western margin was subject to an extensive regime. Therefore, within the West African super continent (Rogers et al., 1995; Dalziel, 1997; Unrug, 1997; Samson and D'Lemos, 1999; Hefferan et al., 2000), the AA is in a position where the main faults acted as wrench faults with respect to the main Pan-African shortening direction (Lapique et al., 1986; Liégeois et al., 1987, 1994; Caby et al., 1989; Caby, 2003). Thus, the AA belt can be considered to have been a transfer zone during Pan-African times (similar to the transpression belt of Ennih and Liégeois, 2001). The abundant evidence for this type of structural behaviour in this area includes the Imiter fault, which evolved from a pure NNW–SSE extensional regime to a NW–SE sinistral transtensional regime (Ouguir et al., 1994; Levresse, 2001). The kinematic characteristics of the other major faults (Central AA fault, SAF, NAF) have not yet been well defined within this late Pan-African framework. Therefore, any attempt to reconstruct the plate tectonic geometry of the Pan-African terranes, and the probable WAC limits that underlie them, would be highly hypothetical.

Acknowledgements

References

Abdesalam, M.G., Liégeois, J-P., Stern, R.J., 2002. The Saharan Metacraton. J. Afr. Earth Sci. 34, 119–136.

Abia, E.H., Nachit, H., Ibhi, H., Baroudi, Z., 1999. Les minéralisations filoniennes à Pb, Zn et Cu de la boutonnière de l'Ougnat. relations avec les déformations et essai de calage chronologique. Chron. Rech. min. 536/537, 137–149.

Abia, E.H., Nachit, H., Marignac, C., Ibhi, A., Aït Saadi, S., 2003. The polymetallic Au–Ag-bearing veins of Bou Madine (Jbel Ougnat, eastern Anti-Atlas, Morocco): tectonic control and evolution of a Neoproterozoic epithermal deposit. J. Afr. Earth Sci. 36, 251–271.

Admou, H., 2000. Structuration de la paléosuture ophiolitique panafricaine de Bou Azzer-Siroua (Anti-Atlas central, Maroc). Unpublished Thesis. University of Marrakech, p. 201.

Aït Isha, M., 1996. Pétrogenèse d'un magmatisme moyennement à fortement potassique. L'exemple du massif panafricain d'Iknioun (Saghro oriental, Anti-Atlas Maroc). Unpublished Thesis. University of Marrakech, p. 243.

Aït Malek, H., 1997. Pétrologie –géochimie et géochronologie U-Pb d'associations acide-basiques: exemples du massif du Velay (Massif Central français) et de l'Anti-Atlas occidental (Maroc). Unpublished Thesis. University of INPL, Nancy, p. 267.

Aït Malek, H., Gasquet, D., Bertrand, J.M., Leterrier, J., 1998. Géochronologie U/Pb sur zircon de granitoïdes éburnéens et panafricains dans les boutonnières protérozoïques d'Igherm, du Kerdous et du Bas Drâa (Anti-Atlas occidental, Maroc). C.R. Acad. Sci. Paris 327, 819–826.

Aït Saadi, 1992. Contribution à l'étude de l'environnement paléovolcanique du Protérozoïque Supérieur (PIII) et du mode de genèse des concentrations polymétalliques (Zn, Pb, Cu, Ag, Au) de Bou Madine (Ougnat, Anti-Atlas oriental, Maroc). Unpublished Thesis. University of INPL, Nancy, p. 218.

Al Ansari, A., Sagon, J.P., 1997. Le gisement d'or de Tiouit (Jbel Saghro, Anti-Atlas) un système mesothermal polyphasé à sulfures- et hématite- or dans une granodiorite potassique d'âge protérozoïque supérieur. Chron. Recher. Min. 527, 3–25.

Amthor, J.E., Grotzinger, J.P., Schröder, S., Bowring, S.A., Ramezani, J., Martin Mark, W., Matter, A., 2003. Extinction of *Cloudina* and *Namacalathus* at the Precambrian–Cambrian boundary in Oman. Geology 31, 431–434.

Azizi Samir, M.R., Ferrandini, J., Tane, J.L., 1990. Tectonique et volcanisme tardi-Pan Africains (580–560 Ma) dans l'Anti-Atlas Central (Maroc): interprétation géodynamique à l'échelle du NW de l'Afrique. J. Afr. Earth Sci. 10, 549–563.

Bajja, A., 2001. Volcanisme syn à post orogénique du Néoprotérozoïque de l'Anti-Atlas: implications pétrogénétiques et géodynamiques. In: De Wall, H., Greiling, R.P. (Eds.), Magmatic evolution of a Neoproterozoic Island-Arc Syn- to Post-orogenic Igneous Activity in the Anti-Atlas (Morocco), vol. 45. Forschunszentrum Jülich Gmbh, pp. 9–228.

Baouch, S., 1984. Etude des ignimbrites et des roches associées du massif de Tichrt (Haut-Atlas, Maroc). Contribution à l'étude du "volcanisme-plutonisme du PIII". Unpublished Thesis, University of Nancy I, p. 131.

Barbey, P., Nachit, H., Pons, J., 2001. Magma–host interactions during differentiation and emplacement of a shallow-level, zoned granitic pluton (Tarçouate pluton, Morocco): implications for magma emplacement. Lithos 58, 125–143.

Barbey, P., Oberli, F., Burg, J.P., Nachit, H., Pons, J., Meier, M., 2004. The Palaeoproterozoic in western Anti-Atlas (Morocco): a clarification. J. Afr. Earth Sci. 39, 239–245.

Barodi, E.B., Maacha, L., Zinbi, Y., 1998. Les minéralisations argentifères au Maroc: cas du gisement d'Imiter. Chron. Rech. Min. 531/532, 77–92.

Barra, F., Ruiz, J., Mathur, R., Titley, S., 2003. A rhenium–osmium study of sulfides from the Bagdad porphyry Cu–Mo deposit, northern Arizona, USA. Miner. Deposita 38, 585–596.

Bassias, Y., Wallbrecher, E., Willgallia, A., 1988. Tectono-thermal evolution of the late Panafrican Orogeny in the central Anti-Atlas; southern Morocco. In: Jacobshagen, V.H. (Ed.), The Atlas System of Morocco, Studies on its Geodynamic Evolution. Lecture Notes Earth Sci., vol. 15, pp. 43–60.

Belfoul, M.A., Faik, F., Hassenforder, B., 2001. Mise en évidence d'une tectonique tangentielle antérieure au plissement majeur dans la chaîne hercynienne de l'Anti-Atlas occidental. Maroc. J. Afr. Earth Sci. 32, 723–739.

Belkabir, A., Maacha, L., Madi, A., Jébrak, M., 2004. Gold-rich roots of Proterozoic ophiolite-hosted volcanogenic massive sulfide deposit, Bleida, Anti-Atlas, Morocco. In: Abstract, 20th Colloquium of African Geology, Orléans, p. 71.

Ben Othman, D., Fourcade, S., Allègre, C.J., 1984. Recycling processes in granite-granodiorite complex genesis: the Quérigut case studied by Nd–Sr isotopic systematics. Earth Planet. Sci. Lett. 69, 290–300.

Benssaou, M., Hamoumi, N., 1999. Paléoenvironnements et minéralisations de l'Anti-Atlas occidental marocain au Cambrien précoce. Chron. Rech. Min. 536/537, 113–120.

Benssaou, M., Hamoumi, N., 2001. L'Anti-Atlas occidental du Maroc: étude sédimentologique et reconstitutions paléogéographiques du Cambrien inférieur. J. Afr. Earth Sci. 3, 351–372.

Benziane, F., Prost, A.E., Yazidi, A., 1983. Le passage du Précambrien au Cambrien précoce volcanique et sédimentaire de l'Anti-Atlas oriental; comparaisons avec l'Anti-Atlas occidental. Bull. Soc. Géol. France 4, 549–556.

Boher, M., Abouchami, W., Michard, A., Albarède, F., Arndt, N., 1992. Crustal growth in West Africa at 2.1 Ga. J. Geophys. Res. 97, 345–369.

Bouougri, E.L., Saquaque, A., 2004. Lithostratigraphic framework and correlation of the Neoproterozoic northern West African Craton passive margin sequence (Siroua–Zenaga–Bouazzer Elgraara Inliers, Central Anti-Atlas, Morocco): an integrated approach. J. Afr. Earth Sci. 39, 227–238.

Brabers, P.M., 1988. A plate tectonic model for the Pan-African Orogeny in the Anti-Atlas, Morocco. In: Jacobshagen, V.H. (Ed.), The Atlas System of Morocco, Studies on its geodynamic Evolution, Lecture Notes Earth Sci., vol. 15, pp. 61–80.

Caby, R., 2003. Terrane assembly and geodynamic evolution of central–western Hoggar: a synthesis. J. Afr. Earth Sci. 37, 133–159.

Caby, R., Andreopoulous-Renaud, U., Pin, C., 1989. Late Proterozoic arc–continent and continent–continent collision in the Pan-African Trans-Saharan belt of Mali. Can. J. Earth Sci. 26, 1136–1146.

Camara, L.S., 1993. Etude cartographique, pétrographique, minéralogique et géochimique des granitoïdes du district minier d'Imiter. Unpublished Thesis. University of Marrakech, p. 143.

Caritg, S., Burkhard, M., Ducommun, R., Helg, U., Kopp, L., Sue, C., 2004. Fold interference patterns in the Late Palæozoic Anti-Atlas belt of Morocco. Terra Nova 16 (1), 27–37.

Chabane, A., 1991. Les roches vertes du Protérozoique supérieur de Khzama (Siroua, Anti-Atlas central, Maroc), un exemple Précambrien d'ophiolite d'avant arc formée en contexte transformant. Unpublished Thesis. University of Marrakech, p. 570.

Chalot-Prat, F., Gasquet, D., Roger, J., Hassenforder, B., Chévremont, P., Baudin, T., Razin, P., Benlakhdim, A., Benssaou, M., Mortaji, A., Mémoire explicatif, carte géol. Maroc (1/50000), Feuille Sidi Bou'addi, Notes et Mémoires Serv. Géol. Maroc, No. 415 bis, MICEM/BRGM. Geological map by Hassenforder, B., Roger, J., Baudin, T., Chalot-Prat, F., Gasquet, D., Berrhama, M., Chévremont, P., Marquer, D., Razin, P., Benlakhdim, A.

Charlot, R., 1976. The Precambrian of the Anti-Atlas (Morocco); a geochronological synthesis. Precamb. Res. 3, 273–299.

Chbani, B., Beauchamp, J., Algouti, A., Zouhair, A., 1999. Un enregistrement sédimentaire éocambrien dans un basin intracontinental en distension: le cycle conglomérats de base-unité calcaire-grés de Tikirt de Bou Azzer EL Graara (Anti-Atlas, Maroc). C.R. Acad. Sci. Paris 329, 317–323.

Cheilletz, A., Gasquet, D., 2001. Specific plate tectonic environments for the Anti-Atlas ore deposits. In: Abstract, 3MA Colloquium, Marrakech, Morocco, p. 84.

Cheilletz, A., Levresse, G., Gasquet, D., Azizi Samir, M.R., Zyadi, R., Archibald, D.A., 2002. The Imiter epithermal deposit (Morocco): new petrographic, microtectonic and geochronological data. Importance of the Precambrian–Cambrian transition for major precious metals deposits in the Anti-Atlas. Miner. Deposita 37, 772–781.

Chen, J.H., Papanastassiou, D.A., Wasserburg, G.J., 1998. Re/Os systematics in chondrites and the fractionation of the platinum group elements in the early solar system. Geochim. Cosmochim. Acta 62, 3379.

Choubert, G., 1952. Le volcan géorgien de la région d'Alougoum (Anti-Atlas). C.R. Acad. Sc., Paris 234 (3), 350–352.

Choubert, G., 1963. Histoire géologique de l'Anti-Atlas de l'archéen à l'aurore des temps primaires. Notes Mém. Serv. géol. Maroc 62, pp. 350–352.

Church, W.R., 1980. Late Proterozoic ophiolites. In: Aubouin, J., Allegre, C.J. (Eds.), Basic–Ultrabasic Associations in Orogenic Belts, vol. 272. Centre National Recherche Scientifique, Paris, pp. 105–118.

Clauer, N., 1974. Utilisation de la méthode Rb-Sr pour la datation d'une schistosité de sédiments peu métamorphisés: applications au Précambrien II de la boutonnière de Bou Azzer–El Graara (Anti-Atlas, Maroc). Earth Planet. Sci. Lett. 22, 404–412.

Clauer, N., 1976. Géochimie isotopique du strontium des milieux sédimentaires: application à la géochronologie de la couverture du craton Ouest-Africain. Sci. Geol. (Strasbourg) 45, 256.

Compston, W., Williams, I.S., Kirschvink, J.L., Zhang, Z., Ma, G., 1992. Zircon U/Pb ages for the early Cambrian timescale. J. Geol. Soc. London 149, 171–184.

Dallmeyer, R.D., Lecorché, J.P., 1991. The West African orogens and circum-Atlantic correlatives. Sringer Verlag, 405 p.

Dalziel, I.W.D., 1997. Neoproterozoic–Palæozoic geography and tectonics: review, hypothesis and environmental speculation. Bull. Geol. Soc. Am. 109, 16–42.

De Wall, H., Kober, B., Errami, E., Greiling, R.O., Ennih, N., 2001. Age and crustal setting of the granitoid emplacement in the area of Imiter (eastern Saghro). In: Abstract, 3MA Colloquium, Marrakech, Morocco, p. 48.

Deloule, E., Alexandrov, P., Cheilletz, A., Laumonier, B., Barbey, P., 2002. In-situ U–Pb zircon ages for early Ordovician magmatism in the eastern Pyrenees, France: the Canigou orthogneisses. Int. J. Earth Sci. 91, 398–405.

Du Dresnay, R., 1976. Carte géologique du haut Atlas d'Anoual–Bou Anane (Haut Atlas oriental) au 1/200 000. Edit. Serv. Géol. Maroc, Notes et Mémoires 246.

Ducrot, J., 1979. Datation à 615 Ma de la granodiorite de Bleida et conséquences sur la chronologie des phases tectoniques, métamorphiques et magmatiques panafricaines dans l'Anti-Atlas marocain. Bull. Soc. Géol. France XXI (4), 495–499.

Ducrot, J., Lancelot, J.R., 1977. Problème de la limite Précambrien–Cambrien: étude radiochronologique par méthode U–Pb sur zircon du Jbel Bobo (Anti-Atlas marocain). Can. J. Earth Sci. 14, 2771–2777.

Eddif, A., 2002. Géochronologie, pétrologie, géochimie et structure des intrusions tardi-panafricaines de Wirgane et de leur couverture néoprotérozoïque à paléozoïque (Haut-Atlas occidental). Unpublished Thesis. University of Rabat, p. 194.

Eddif, A., Gasquet, D., Hoepffner, C., Aït Ayad, N., 2000. Les intrusions de Wirgane (Haut Atlas occidental): témoins d'un magmatisme hercynien syn à tardi-cinématique? J. Afr. Earth Sci. 31, 483–498.

El Aouli, E.H., Gasquet, D., Ikenne, M., 2001. Le magmatisme basique de la boutonnière d'Igherm (Anti-Atlas occidental, Maroc): un jalon des distensions néoprotérozoïques sur la bordure nord du craton ouest africain. Bull. Soc. Géol. France 3, 309–317.

El Boukhari, A., Chabane, A., Rocci, G., Tane, J.L., 1991. Le volcanisme de la région de N'Kob (SE du Siroua, Anti-Atlas Marocain) témoin de l'existence d'un rift au Protérozoïque supérieur, à la marge NE du Craton ouest africain. C.R. Acad. Sci. Paris 312 (Série II), 735–738.

En-Naciri, A., Barbanson, L., Touray, J.C., 1997. Brine inclusions from the Co–As(Au) Bou Azzer district, Anti-Atlas mountains, Morocco. Econ. Geol. 92, 360–367.

Ennih, N., Liégeois, J.P., 2001. The Moroccan Anti-Atlas: the West African craton passive margin with limited Pan-African activity. implications for the northern limit of the craton. Precamb. Res. 112, 289–302.

Ennih, N., Liégeois, J.P., 2003. The Moroccan Anti-Atlas: the West African craton passive margin with limited Pan-African activity.

Implications for the northern limit of the craton: reply to comments by E. H. Bouougri Precambr. Res. 120, 185–189.

Esser, B., Turekian, K., 1993. The Osmium isotopic composition of the continental crust. Geochim. Cosmochim. Acta 57, 3093–3104.

Evensen, N.M., Hamilton, P.J., O'Nions, R.K., 1978. Rare earth abundances in chondritic meteorites. Geochim. Cosmochim. Acta 42, 1199–1212.

Faure, G., 2001. Origin of igneous rocks. In: The Isotopic Evidence. Springer, Berlin, p. 494.

Fekkak, A., Boualoul, M., Badra, L., Amenzou, M., Saquaque, A., El Amrani, I.E., 1999. Origine et contexte géotectonique des dépôts détritiques du Groupe néoprotérozoique inférieur de Kelaat Mgouna (Anti-Atlas oriental, Maroc). J. Afr. Earth Sci. 30, 295–311.

Fekkak, A., Pouclet, A., Benharref, M., 2003. The Middle Neoproterozoic Sidi Flah Group (Anti-Atlas, Morocco): synrift deposition in a Pan-African continent/ocean transition zone. J. Afr. Earth Sci. 37, 73–87.

Fekkak, A., Pouclet, A., Ouguir, H., Ouazzani, H., Badra, L., Gasquet, D., 2001. Géochimie et signification géotectonique des volcanites du Cryogénien inférieur du Saghro (Anti-Atlas oriental, Maroc). Geodinam. Acta 14 (6), 373–385.

Frei, R., Nägler, Th.F., Schönberg, R., Kramers, J.D., 1998. Re–Os, Sm–Nd, U–Pb and stepwise Pb leaching isotope systematics in shear-zone hosted gold mineralization; genetic tracing and age constraints of crustal hydrothermal activity. Geochim. Cosmochim. Acta 62, 1925–1936.

Freton, R., 1988. Contribution à l'étude métallogénique du district de Bou Madine (Anti-Atlas, Maroc): environnement tectonique et concentrations épithermales B.P.G.C. à Ag et Au. Unpublished Thesis. University of INPL, Nancy, p. 246.

Frost, B.R., Barnes, C.G., Collins, W.J., Arculus, R.J., Ellis, D.J., Frost, C.D., 2001. A geochemical classification for granitic rocks. J. Petrol. 42, 2033–2048.

Gasquet, D., Chèvremont, P., Baudin, T., Chalot-Prat, F., Guerrot, C., Cocherie, A., Roger, J., Hassenforder, B., Cheilletz, A., 2004. Polycyclic magmatism in the Tagragra and Kerdous-Tafeltast inliers (Western Anti-Atlas, Morocco). J. Afr. Earth Sci. 39, 267–275.

Gasquet, D., Roger, J., Chalot-Prat, F., Hassenforder, B., Baudin, T., Chévremont, P., Razin, P., Benlakhdim, A., Mortaji, A., Benssaou, M., 2001. Mémoire explicatif, carte géol. Maroc (1/50000), Feuille Tamazrar, Notes et Mémoires Serv. Géol. Maroc, No. 415 bis, MICEM/BRGM. Geological map by Roger, J., Gasquet, D., Baudin, T., Chalot-Prat, F., Hassenforder, B., Marquer, D., Chevremont, P., Berrhama, M., Destombes, J., Razin, P., Benlakhdim, A.

Gradstein, F., Ogg, J.G., Smith, A.G., Bleeker, W., Lourens, L.J., 2004. A new geologic time scale, with special reference to Precambrian and Neogene. Episodes 27 (2), 83–100.

Hassenforder, B., 1987. La tectonique panafricaine et varisque de l'Anti-Atlas dans le massif du Kerdous, Maroc. Thèse Doctorat ès-Sciences. Université Louis Pasteur, Strasbourg, p. 249.

Hefferan, K., Karson, J.A., Saquaque, A., 1992. Proterozoic collisional basins in a Pan-African suture zone, Anti-Atlas Mountains, Morocco. Precamb. Res. 54, 295–319.

Hefferan, K.P., Admou, H., Hilal, R., Karson, J.A., Saquaque, A., Juteau, T., Bohn, M., Samson, S.D., Kornprobst, J., 2002. Proterozoic blueschist-bearing mélange in theAnti-Atlas Mountains, Morocco. Precamb. Res. 118, 179–194.

Hefferan, K.P., Admou, H., Karson, J.A., Saquaque, A., 2000. Anti-Atlas (Morocco) role in Neoproterozoic Western Gondwana reconstruction. Precamb. Res. 103, 89–96.

Helg, U., Burkhard, M., Caritg, S., Robert-Charrue, C., 2004. Folding and inversion tectonics in the Anti-Atlas of Morocco. Tectonics 23, TC4006, doi: 10.1029/2003T001576.

Houari, M.R., Hoepffner, C., 2003. Late Carboniferous dextral wrench-dominated transpression along the North African craton margin (Esatern High-Atlas, Morocco). J. Afr. Earth Sci. 37, 11–24.

Huch, K.M., 1988. Die panafrikanische Khzama-Geosutur im zentralen Anti-Atlas. Petrpographie, Geochemie und Geochronologie des Subduktionskomplexes der Tourtit-Ophiolithe und der Tachoukacht-Gneise sowie einiger Kollisionsgesteine im Nordosten des Sirwa-Kristallindoms. Verlag Schelzky & Jeep, 172 pp.

Ighid, L., Saquaque, A., Reuber, I., 1989. Plutons syncinématiques et la déformation panafricaine majeure dans le Saghro oriental (Boutonnière d'Imiter, Anti-Atlas, Maroc). C.R. Acad. Sci., Paris IIa 309, 615–620.

Ikenne, M., 1997. La boutonnière précambrienne du bas Draa (Anti-Atlas occidental, Maroc): caractérisation pétrologique et géochimique des roches magmatiques et métamorphiques et leurs relations avec la déformation. Unpublished Thesis. University of Agadir, p. 259.

Inglis, J.D., MacLean, J.S., Samson, S.D., D'Lemos, R.S., Admou, H., Hefferan, K., 2004. A precise U-Pb zircon age for the Bleida granodiorite, Anti-Atlas, Morocco: implications for the timing of deformation and terrane assembly in the eastern Anti-Atlas. J. Afr. Earth Sci. 39, 277–283.

Juery, A., 1976. Datation U–Pb du socle précambrien du Haut-Atlas (Maroc). Unpublished Thesis. University of Paris, p. 85.

Karl, A., de Wall, H., Rieger, M., Schmitt, T., Errami, E., Kober, B., Greiling, R.O., 2001. Petrography and geochemistry of the Bou Teglimt, Taouzzakt and Igoudrane intrusions in the Eastern Saghro (Anti-Atlas, Morocco). In: De Wall, H., Greilling, R.P. (Eds.), Magmatic evolution of a Neoproterozoic Island-Arc Syn-To Post-orogenic Igneous Activity in the Anti-Atlas (Morocco) Forschunszentrum Jülich Gmbh, vol. 45, pp. 243–254.

Kay, S.M., Mpodozis, C., 2001. Central Andean ore deposits linked to evolving shallow subduction systems and thickening crust. GSA Today 11 (3), 4–9.

Kearey, P., Vine, F.J., 1992. Global Tectonics. Blackwell Scientific Publications, Oxford, p. 302.

Landing, E., Bowring, S.A., Davidek, K.L., Westrop, S.R., Geyer, G., Heldmaier, W., 1998. Duration of the Early Cambrian: U–Pb ages of volcanic ashes from Avalon and Gondwana. Can. J. Earth Sci. 35, 329–338.

Lapique, F., Bertrand, J.M., Meriem, D., 1986. A major Pan-African crustal decoupling zone in the Timgaouine area (Western Hoggar, Alageria). J. Afr. Earth Sci. 5, 617–625.

Le Maitre, R.W., Bateman, P., Dudek, A., Keller, J., Lameyre, J., Le Bas, M.J., Sabine, P.A., Schmid, R., Sorensen, H., Streckeisen, A., Wooley, A.R., Zanettin, B., 1989. Classification of Igneous Rocks and Glossary of Terms. Blackwell, Oxford.

Leblanc, M., 1975. Ophiolites précambriennes dans le PII de l'Anti-Atlas central (Maroc). Unpublished Thesis. University of Paris VI, p. 329.

Leblanc, M., 1981. Ophiolites précambriennes et gîtes arséniés de cobalt (Bou-Azzer, Maroc). Notes Mém. Serv. Géol. Maroc 280, p. 306.

Leblanc, M., Lancelot, J., 1980. Interprétation géodynamique du domaine panafricain de l'Anti-Atlas (Maroc) à partir de données géologiques et géochronologiques. Can. J. Earth Sci. 17, 142–155.

Leblanc, M., Moussine-Pouchkine, A., 1994. Sedimentary and volcanic evolution of a Neoproterozoic continental margin. Precamb. Res. 70, 25–44.

Lebrun, J., 1982. Etude du volcanisme précambrien de la région d'Issougrid (Ouarzazarte, Maroc) et des minéralisations cuprifères associées. Unpublished Thesis. University of Paris-Sud Orsay, p. 376.

Leistel, J.M., Qadrouci, A., 1991. Le gisement argentifère d'Imiter (protérozoïque supérieur de l'Anti-Atlas, Maroc). Contrôles des minéralisations, hypothèse génétique et perspectives pour l'exploration. Chron. Rech. Min. 502, 5–22.

Levresse, G., 2001. Contribution à l'établissement d'un modèle génétique des gisements d'Imiter (Ag–Hg) Bou Madine (Pb–Zn–Cu–Au) et Bou Azzer (Co–Ni–As–Au–Ag) dans l'Anti-Atlas marocain. Unpublished Thesis. University of INPL, Nancy, p. 191.

Levresse, L., Cheilletz, A., Gasquet, D., Reisberg, L., Deloule, E., Marty, B., Kyser, K., 2004. Osmium, sulphur, and helium isotopic results from the giant Neoproterozoic epithermal Imiter silver deposit, Morocco: evidence for a mantle source. Chem. Geol. 207, 59–79.

Liégeois, J.P., Bertrand, J.M., Black, R., 1987. The subduction- and collision-related Pan-African composite batholith of the Adrar des Iforas (Mali): a review. Geol. J. 22, 185–211.

Liégeois, J.P., Black, R., Navez, J., Latouche, L., 1994. Early and late Pan-African orogenies in the Air assembly of terranes (Tuareg Shield, Niger). Precamb. Res. 67, 59–88.

Ludwig, K.R., 2003. Users Manual for Isoplot/Ex Version 3.00: a Geochronological Toolkit for Microsoft Excel (Special Publication), vol. 4. Geochronology Center, Berkeley, pp. 1–71.

Maacha, L., Azizi-Samir, M.R., Bouchta, R., 1998. Gisements cobaltifères du district de Bou Azzer (Anti-Atlas): structure et conditions de genèse. Chron. Rech. Min. 531/532, 65–75.

Magaritz, M., Kirschvink, J.L., Latham, A.J., Zhuravlev, A.Y., Rozanov, A.Y., 1991. Precambrian/Cambrian boundary problem: carbon isotope correlations for Vendian and Tommotian time between Siberia and Morocco. Geology 19, 847–850.

Marini, F., Ouguir, H., 1990. Un nouveau jalon dans l'histoire de la distension pre-panafricaine au Maroc: le Precambrien II des boutonnières du Jbel Saghro nord-oriental (Anti-Atlas, Maroc). C.R. Acad. Sci. Paris 310, 577–582.

Mathur, R., Ruiz, J., Munizaga, F., 2000a. Relationship between copper tonnage of Chilean base–metal porphyry deposits and Os isotope ratios. Geology 28, 555.

Mathur, R., Ruiz, J., Herb, P., Hahn, L., Burgath, K.P., 2003. Re–Os isotopes applied to the epithermal gold deposits near Bucaramanga, northeastern Colombia. J. South Am. Earth Sci. 15 (7), 815–821.

Mathur, R., Ruiz, J., Titley, S., Gibbins, S., Margotomo, W., 2000b. Different crustal sources for Au-rich and Au-poor ores of the Grasberg Cu–Au Porphyry Deposit. Earth Planet. Sci. Lett. 183, 7–14.

Michard, A., Gurriet, P., Soudant, M., Albarède, F., 1985. Nd isotopes in French Phanerozoic shales: external vs. internal aspects of crustal evolution. Geochim. Cosmochim. Acta 49, 601–610.

Mifdal, A., Peucat, J.J., 1985. Datations U/Pb et Rb/Sr du volcanisme acide de l'Anti-Atlas marocain et du socle sous-jacent dans la région de Ouarzazate. Apport au problème de la limite Précambrien–Cambrien. Sci. Géol. Bull. 38, 185–200.

Mokhtari, A., 1993. Nouvelles données et interprétations du massif basique de Tagmout (Jbel Saghro, Anti-Atlas, Maroc): relations avec les granitoïdes associés. Unpublished Thesis. University of Nancy I, p. 251.

Mouttaqi, A., 1997. Hydrothermalisme et minéralisations en relation avec le rifting protérozoïque supérieur: exemple du gisement de cuivre de Bleida (Anti-Atlas), Maroc. Unpublished Thesis. University of Marrakech, Maroc, p. 310.

Mrini, Z., 1993. Chronologie (Rb–Sr, U–Pb), traçage isotopique (Sr–Nd–Pb) des sources des roches magmatiques éburnéennes, panafricaines et hercyniennes du Maroc. Unpublished Thesis. University of Marrakech, Marocm p. 227.

Murphy, J.B., 2002. Geochemistry of the Neoproterozoic metasedimentary Gamble Brook Formation, Avalon Terrane, Nova Scotia: evidence for a rifted-arc environment along the West Gondwanian margin of Rodinia. J. Geol. 110, 407–419.

Murphy, J.B., Nance, R.D., 1989. Model for the evolution of the Avalonian–Cadomian belt. Geology 17, 737–738.

Murphy, J.B., Nance, R.D., 2002. Sm–Nd isotopic systematics as tectonic tracers: an example from West Avalonia in the Canadian Appalachians. Earth Sci. Rev. 59, 77–100.

Neves, S.P., 2003. Proterozoic history of the Borborema province (NE Brazil): correlations with neighboring cratons and Pan-African belts and implications for the evolution of western Gondwana. Tectonics 22 (4), 1031.

Ord, A., Walshe, J.L., Hobbs, B.E., 1999. Geodynamics and giant ore deposits. In: Stanley, et al. (Ed.), Mineral Deposits: Processes to Processing. Balkema, Rotterdam, pp. 1341–1344.

Ouazzani, H., Pouclet, A., Badra, L., Prost, A., 2001. Le volcanisme d'arc du massif ancien de l'Ouest du Haut-Atlas occidental (Maroc), un témoin de la convergence de la branche occidentale de l'océan panafricain. Bull. Soc. Géol. France 172, 587–602.

Oudra, M., Gasquet, D., Hassenforder, B., Ikenne, M., 2003. Pan-African tectonics in the Igherm area (western Anti-Atlas, Morocco): consequences on the Neoproterozoic evolution of the NW border of the Wesrtern African craton. In: Abstract, First Meeting of IGCP 485-El Jadida, Morocco, December 1–2, 2003, p. 51.

Ouguir, H., 1997. Contexte géologique du gisement argentifère d'imiter (Anti-Atlas oriental, Maroc). Contrôle volcanique et structural de la mise en place des concentrations métalliques à Ag–Hg. Unpublished Thesis. University of Meknès, p. 215.

Ouguir, H., Macaudière, J., Dagallier, G., Qadrouci, A., Leistel, J.M., 1994. Cadre structural du gîte Ag–Hg d'Imiter (Anti-Atlas, Maroc): implications métallogéniques. Bull. Soc. Géol. France 165, 233–248.

Ouguir, H., Macaudière, J., Dagallier, G., 1996. Le protérozoïque supérieur d'Imiter, Saghro oriental, Maroc: un contexte géodynamique d'arrière-arc. J. Afr. Earth Sci. 22, 173–189.

Piqué, A., 1994. Géologie du Maroc. In: Les domaines régionaux et leur évolution structurale. PUMAG, Rabat, p. 284.

Piqué, A., 2003. Evidence for an important extensional event during the Latest Proterozoic and Earliest Palaeozoic in Morocco. C.R. Geosci. 335, 865–868.

Pomerol, C., Lagabrielle, Y., Renard, M., 2005. Eléments de Géologie, 13th ed. Dunod, Paris, p. 629.

Rogers, J.J.W., Unrug, R., Sultan, M., 1995. Tectonic assembly of Gondwana. J. Geodyn. 19, 1–34.

Samson, R.D., D'Lemos, R.S., 1999. A precise Late Neoproterozoic U–Pb zircon age for the syntectonic Perelle quartz diorite, Guernsey, Channel Islands, UK. J. Geol. Soc. London 156, 47–54.

Samson, S.D., Inglis, J.D., D'Lemos, R.S., Admou, H., Blichert-Toft, J., Hefferan, K., 2003. U–Pb age, geochemistry, and Nd–Hf isotopic composition of Neoproterozoic plagiogranites within the Tasriwine Ophiolite, Siroua inlier, Anti-Atlas orogen, Morocco. In: Abstract, First Meeting of IGCP 485-El Jadida, Morocco, December 1–2, 2003, pp. 64–68.

Saquaque, A., Admou, H., Karson, J., Hefferan, K., Reuber, I., 1989. Precambrian accretionary tectonics in the Bou Azzer–El Graara region. Anti-Atlas, Morocco. Geology 17, 1107–1110.

Saquaque, A., Benharref, M., Abia, H., Mrini, Z., Reuber, I., Karson, J., 1992. Evidence for a Pan-African volcanic arc and wrench fault tectonics in the Jbel Saghro, Anti-Atlas, Morocco. Geol. Rundsch. 81, 1–13.

Shen, J.J., Yang, H.J., 2004. Sources and genesis of the Chinkuashih Au-Cu deposits in northern Taiwan: constrains from Os and Sr isotopic compositions of sulfides. Earth Planet. Sci. Lett. 222, 71–83.

Soulaïmani, A., Le Corre, Cl., Farazdaq, R., 1997. Déformation hercynienne et relation socle/couverture dans le domaine du Bas-Drâa (Anti-Atlas occidental, Maroc). J. Afr. Earth Sci. 24 (3), 271284.

Soulaimani, A., Piqué, A., 2004. The Tasrirt structure (Kerdous inlier, Western Anti-Atlas, Morocco): a late Pan-African transtensive dome. J. Afr. Earth Sci. 39, 247–255.

Soulaïmani, A., Piqué, A., Bouabdelli, M., 2001. La série du PII–III de l'Anti-Atlas occidental (Sud marocain): un olistostrome à la base de la couverture post-panafricaine (PIII) du Protérozoïque supérieur. C.R. Acad. Sci. Paris 332, 121–127.

Thomas, R.J., Chevallier, L.P., Gresse, P.G., Harmer, R.E., Eglington, B.M., Armstrong, R.A., de Beer, C.H., Martini, J.E.J., de Kock, G.S., Macey, P.H., Ingram, B.A., 2002. Precambrian evolution of the Sirwa Window, Anti-Atlas Orogen, Morocco. Precamb. Res. 118, 1–57.

Thomas, R.J., De Beer, C.H., Chevallier, L.P., De Kock, G.S., Gresse, P.G., 2000. Notice Explicative de la Carte Géologique du Maroc au 1/50000 feuille Assarag. Notes et Mémoires Serv. Geol. Maroc 392, p. 84.

Thomas, R.J., Fekkak, A., Ennih, N., Errami, E., Loughlin, E.S., Gresse, P.G., Chevallier, L.P., Liegeois, J.P., 2004. A new lithostratigraphic framework for the Anti-Atlas orogen, Morocco. J. Afr. Earth Sci. 39, 217–226.

Unrug, R., 1997. Rodinia to Gondwana: the geodynamic map of Gondwana supercontinent assembly. GSA Today 7, 1–5.

Viland, J.C., 1988. Le cuivre et les métaux associés de l'Anti-Atlas marocain. Notes Mem. Serv. Géol. Maroc 334, 127–213.

Villeneuve, M., Cornée, J.J., 1994. Structure, evolution and paleogeography of the West African craton and bordering belts during the Neoproterozoic. Precamb. Res. 69, 307–326.

Walsh, G.J., Aleinikoff, J., Benziane, F., Yazidi, A., Amstrong, T.R., 2002. U-Pb zircon geochronology of the Palæoproterozoic Tagragra de Tata inlier and its Neoproterozoic cover, western Anti-Atlas, Morocco. Precamb. Res. 117, 1–20.